The Cryosphere Discuss., https://doi.org/10.5194/tc-2017-253
Manuscript under review for journal The Cryosphere
Discussion started: 22 December 2017
© Author(s) 2017. CC BY 4.0 License.

The Cryosphere Discussions
Open Access
EGU

Melting over the East Antarctic Peninsula (1999-2009): evaluation of a high-resolution regional climate model

Rajashree T. Datta[1], Marco Tedesco[2], Cecile Agosta[3], Xavier Fettweis[3], Peter Kuipers Munneke[4], Michiel R. van den Broeke.[4]

[1]The Graduate Center, City University of New York, NY 10016, USA
[2]Lamont-Doherty Earth Observatory of Columbia University, Palisades, New York, New York 10964, USA
[3]Department of Geography, Université de Liège, Liège, Belgium
[4]Institute for Marine and Atmospheric Research, Utrecht University, Utrecht, The Netherlands

Correspondence to: Rajashree Tri Datta (Tri.Datta@gmail.com)

Abstract. Surface melting over the Antarctic Peninsula (AP) plays a crucial role for the stability of ice shelves and dynamics of grounded ice, hence modulating the mass balance in a region of the world which is particularly sensitive to increasing surface temperatures. Understanding the processes that drive melting using surface energy and mass balance models is fundamental to improving estimates of current and future surface melting and associated sea level rise through ice-shelf collapse. This is even more important in view of the specific challenges presented by how circulation patterns over the topographically-complex Antarctic Peninsula, especially föhn winds, impact surface melt. In this study, we evaluate the regional climate model Modèle Atmosphérique Régionale (MAR) over the Antarctic Peninsula (AP) at a 10 km spatial resolution between 1999 and 2009, a period which coincides with the availability of active microwave data from the QuikSCAT mission. This is the first time that this model, which has been validated extensively over Greenland, has been applied to the Antarctic Peninsula at a high resolution. Our primary regional focus is the northern East Antarctic Peninsula (East AP), where we define smaller sub-regions according to divergent melt occurrence biases. Melting in the East AP can be initiated both by sporadic westerly föhn flow over the AP and by northerly winds advecting warm air from lower latitudes. To assess MAR's ability to simulate these physical processes, this study takes a unique approach, examining model biases for melt occurrence on the Larsen Ice Shelf, as evaluated by satellite estimates from passive and active microwave data, with concurrent temperature biases associated with wind direction biases as evaluated by three automatic weather stations (AWS). Our results indicate that satellites estimates show greater melt frequency, a larger melt extent, and a quicker expansion to peak melt extent than MAR in the center and east of the Larsen C ice shelf. The difference between the remote sensing and modeled estimates reduces in the north and west of the East AP. Our results indicate that although MAR shows an overall warm bias, it also shows fewer warm, strong westerly winds than reported by AWS stations, which may lead to an underestimation of melt. The underestimation of föhn flow in the east of the Larsen C may potentially be resolved by removing the hydrostatic assumption in MAR or increasing spatial resolution. The underestimation of southwesterly flow in particular may be reduced by using higher-resolution topography.

The Cryosphere Discuss., https://doi.org/10.5194/tc-2017-253
Manuscript under review for journal The Cryosphere
Discussion started: 22 December 2017
© Author(s) 2017. CC BY 4.0 License.

1 Introduction

Increased meltwater production over the Antarctic Peninsula (AP) in the latter half of the 20th century has been linked to a warming atmosphere, with potential implications for future sea-level rise (Barrand et al., 2013; Turner et al., 2005; Vaughan, 2006). Surface melting has been implicated in the weakening and eventual collapse of ice shelves as well as the subsequent acceleration of contributing glaciers, with the Larsen A (1995) and Larsen B (2002) on the East AP as the most notable examples (Vaughan et al, 1996; Rott et al, 1998; Scambos, 2004). In July 2017, a rift on the Larsen C Ice Shelf, which had been expanding for several years, finally resulted in the calving of the 5800 km^2 iceberg A68.

Surface melting influences ice shelf stability through the stress produced by melt ponding as well as percolation through firn. One proposed mechanism for the disintegration of ice shelves hypothesizes that surface meltwater infills and deepens pre-existent crevasses, through a process called hydrofracture (Scambos et al., 2000; Weertman, 1973; van der Veen et al., 1997). In addition, a complementary mechanism proposes that when supraglacial lakes drain (becoming dolines), an upward flexure is induced which can weaken an ice shelf, both at the surface and at the base (MacAyeal and Sergienko, 2013). Large open-rift systems were observed over the Larsen B ice shelf in the summer of 2002 which are consistent with substantial melt initiating both mechanisms and leading to ice shelf disintegration (Glasser et al.,2008; MacAyeal and Sergienko, 2013). Alternatively, meltwater can affect ice shelf dynamics by percolating into firn and increasing its density until no air remains. In the absence of pore space, meltwater moves through the underlying ice sheet or collects on the surface in melt ponds. This process, operating over decades, can therefore pre-condition the ice sheet for both hydrofracture and post-drainage flexure stress during high-melt seasons (Kuipers Munneke et al., 2014). Meltwater can also form under blue ice surfaces, likely due to smaller extinction coefficients and lowered albedo of ice (Brandt and Warren 1993) as well as under low-density snow on clear days when temperatures are slightly below freezing (Koh and Jordan 1995). Modeling studies suggested that the different sensitivities of blue-ice vs subsurface snow melt is a product of the radiative and heat transfer interactions resulting from their differing albedo, grain size and density (Liston et al,, 1999a; Liston et al.1999b). The net effects of melt over blue ice flowing downstream in subsurface layers (the ice-albedo feedback) has recently been shown to be substantial in parts of East Antarctica (Lenaerts et al., 2016). Recent work has also shown the lateral flow of meltwater (surface rivers) on the Larsen A Ice Shelf in 1979 (Kingslake et al., 2017) which imply prolonged periods of lowered albedo. These surface rivers could be much more prevalent across Antarctica in future warming scenarios than previously expected, and may provide a means of stabilizing ice shelves by routing meltwater away (Bell et al., 2017).

Since the collapse of Larsen A and Larsen B ice shelves, ice velocities of several of their feeding glaciers have increased, and seasonal variations in flow have suggested that both summer meltwater percolation (Zwally, 2002) and the removal of backstress played a role (Scambos, 2004; Rott et al., 2002). The remaining Larsen C ice shelf to the south could prove to be similarly vulnerable to collapse due to atmospheric warming (Morris and Vaughan, 2013). Radar analysis over a 15 year period has shown that Larsen C has been lowering from both firn air depletion (due to either limited accumulation or high surface melt) and basal ice loss, although the latter term is thought to be more substantial (Holland, 2015). While RCMs such as MAR do not account for englacial flow or

The Cryosphere Discuss., https://doi.org/10.5194/tc-2017-253
Manuscript under review for journal The Cryosphere
Discussion started: 22 December 2017
© Author(s) 2017. CC BY 4.0 License.

surface rivers, accurate models of surface meltwater production are a crucial step in assessing the potential effects on the ice sheet, especially in the Larsen C ice shelf.

The East AP, where Larsen C Ice shelf is located, is on average 3-5°C cooler than the West AP at the same latitude (Morris and Vaughan, 2013). This is primarily caused by more exposure to open water in combination with prevailing westerly winds on the west AP and southerly winds on the east AP. Moreover, when strong westerly winds cross the bisecting mountain range of the AP (Fig. 1), the resulting föhn winds can produce pulses of warming on the East Antarctic Peninsula's ice shelves (Marshall, 2007). Föhn winds are a warm, dry air flow on the lee slopes of a mountain range (Beran 1967). This resultant warming can be produced by four main mechanisms. Elvidge (2016) uses a modeling approach to trace four physical processes that occur during föhn flow in the East AP, namely *isentropic drawdown* (sourcing of föhn air from higher altitudes), *latent heating* and *precipitation* (where cooling during uplift on the windward side promotes precipitation), *mechanical mixing* (turbulent sensible heating and drying of low-level flow) and *radiative heating* (where cloudless conditions on the lee side increase the availability of shortwave radiation for heating). The relative importance of each of these mechanisms for surface melt has been shown to be related to the source of föhn flow in the East AP (Elvidge et al., 2015; Grosvenor et al., 2014). For example, southwesterly föhn jets descending from gap flow (from lower-elevation passages in the mountain range) have been shown to be cooler and moister than surrounding föhn flow descending from higher elevations (Elvidge et al., 2015). Recent warming in the East AP has been linked to an increase in föhn winds during recent warming (Cape et al., 2015), which were possibly related to an increase in the speed of warm northwesterly winds which have been associated with positive phases of the Southern Annular Mode (SAM), (Van den Broeke and Van Lipzig, 2003). Because melt in the East AP is as vulnerable to wind dynamics as it is to regional temperature changes, an accurate depiction of föhn flow is crucial for accurate estimates of meltwater production.

Models are limited by the parameterization of physics and our understanding of the physical processes driving the observed changes. RCMs such as the Modèle Atmosphérique Régionale (MAR), evaluated here, can be used for simulating the coupled atmosphere/surface system at a continental and decadal scale (Gallée and Schayes, 1994). The tradeoff, in this case, is that RCMs might not be able to capture physical processes with the required accuracy and must be evaluated alongside observations. Several studies have used passive microwave estimates for melt occurrence alongside *in- situ* temperature data, reporting an increase of surface melting over the AP (Torinesi et al., 2003; Liu et al., 2003; Ridley, 1993; Tedesco et al., 2007; Tedesco et al 2009; Tedesco and Monaghan, 2009). Melt occurrence over the AP has also been investigated using QuikSCAT satellite product at a ~2.225 km resolution (Long and Hicks, 2010) in combination with model outputs from the RCM RACMO (Regional Atmospheric Climate Model) and *in-situ* temperature estimates (Barrand et al., 2013). Raw backscatter values from QuikSCAT have also been used to estimates melt flux over the AP (Trusel et al., 2013; Trusel et al., 2012). A recent study using 5.5km horizontal resolution run of RACMO 2.3 over the AP and focusing on overall surface mass balance (SMB) suggested that a further increase in resolution would be required to properly resolve föhn winds, which would imply the removal of the hydrostatic assumption (Van Wessem et al., 2015). We note, however, that where the hydrostatic assumption is preserved (as with this model run), higher resolutions may inhibit flow in the model, resulting in limited eastward föhn flow in the East AP (Hubert Gallée, personal communication). Observation-based studies on

© Author(s) 2017. CC BY 4.0 License.

the formation of melt ponds in the Cabinet Inlet portion of the Larsen C Ice Shelf have focused on the response to föhn winds (Luckman et al., 2014) and the formation of subsurface ice (Hubbard et al., 2016). These last studies taken together discuss both the atmospheric drivers for melt as well as the effects on the ice shelf within our region of interest, but are necessarily limited to a small region where observations are available. By contrast, spaceborne satellites allow us to estimate surface melt occurrence and meltwater production over the entire AP, complementing *in-situ* data. The combination of satellite-based and *in situ* data provide an excellent toolset for model validation.

Here, we assess the MAR model at a 10 km horizontal spatial resolution over the Antarctic Peninsula, using both satellite and *in-situ* data, aggregating meltwater production to drainage systems (basins) as described by Zwally (2002). While previous studies have evaluated how surface melt is modelled using satellite data, or evaluated the representation of the near-surface atmosphere with AWS data, we use both sources in conjunction (and co-temporally) to understand MAR's ability to simulate specific physical processes, i.e. to assess melt and temperature biases by wind direction. We evaluate surface melt occurrence from MAR at the sub-basin scale using satellite estimates and link melt occurrence biases to temperature and wind biases at a point scale using automatic weather station (AWS) data. We first compare meltwater occurrence derived from two satellite sources with MAR outputs over the Antarctic Peninsula (Sect 3.1). We focus primarily on the NE basin in the East AP as it contains the former Larsen A, Larsen B and current Larsen C Ice Shelf, where three AWS stations are located. In this basin, we define sub-regions based on high and low melt occurrence estimated by three different passive microwave (PMW) algorithms (Tedesco, 2009). We then compare climatologies of melt extent, as well as inter-annual trends, from both passive and active microwave data with those computed from MAR outputs (Sect 3.2). Because melt on the Larsen C Ice Shelf can potentially be initiated by northwesterly fohn flow sourced from over the AP or southwesterly flow through gaps in the mountain range (even at sub-zero temperatures), we compare melt occurrence reported by satellite estimates vs MAR (coinciding with the 2000-2009 QuikSCAT period) partitioned by temperature differences and wind direction. Two additional stations (AWS14 and AWS15) are used to examine the persistence of these wind bias trends to 2014 (Sect. 4). Discussion and conclusions follow in Sect. 5.

2. Data and Methods

This study takes a combined approach, using both model results and observations. The primary tool used to understand the coupled atmosphere and snowpack is the Modèle Atmosphérique Régionale (MAR) RCM. We employ *in-situ* data collected from 3 automatic weather stations (AWS) to evaluate the near-surface atmosphere biases in MAR as well as to assess inter-annual trends. While in-situ observations of 2m air temperature are frequently treated as a proxy for melt (Braithwaite 1981), this method is most effective when the energy budget is dominated by the turbulent sensible heat flux and incoming longwave radiation and does not capture melt which can occur due to shortwave radiative forcing when temperatures are below 0°C (Hock, 2005). Accordingly, we use observations from the QuikSCAT (QS) and SSMR (Scanning Microwave Multichannel Radiometer, 1978-1987) / SSM/I (Special Sensior Microwave/Imager, 1987 - to date) satellites to evaluate both melt occurrence and intensity in MAR.

The Cryosphere Discuss., https://doi.org/10.5194/tc-2017-253
Manuscript under review for journal The Cryosphere
Discussion started: 22 December 2017
© Author(s) 2017. CC BY 4.0 License.

2.1 The Modèle Atmosphérique Régionale (MAR) regional climate model

The Modèle Atmosphérique Régionale (MAR) RCM is a modular atmospheric model coupled to the Soil Ice Snow Vegetation Atmosphere Transfer scheme (SISVAT) surface model (De Ridder and Gallée, 1998), which includes the multi-layer snow model Crocus (Brun et al., 1999). MAR was originally implemented to simulate energy and mass balance processes over Antarctica (Gallée and Schayes, 1994). Within SISVAT, meltwater is calculated at the surface when there is a surplus of energy (a deficit results in refreeze). The presence of meltwater alters the snow history (for example, the type of snowgrains) and percolation through the snowpack is determined through a tipping bucket method based on snow density. A diagram and description of the sequence of these specific processes in MAR is provided in Supplemental Figure 1.

The model configuration used in this study is MAR version 3.5.2, with 23 sigma layers. The snowpack is represented by 30 layers of variable thickness from the surface to a 20 m depth (below which ice is assumed present). The snowpack is initialized at 300 kg/m^3 at the surface and 600 km/m^3 at depth. Following 2 years of spinup, MAR results are independent of the initial conditions ; this model run had a spin-up of 5 years for each final model year.

For the purposes of this study, MAR outputs are generated at a horizontal spatial resolution of 10 km for the years between 1999 and 2014. Lateral boundary conditions are specified from the European Centre for Medium-Range Weather Forecasts, using the ERA-Interim reanalysis (Dee et al., 2011). We note that the mask used does not include the Larsen A or Larsen B Ice Shelf in order to preserve consistency for comparison between years (most of which post-date the collapse of these ice shelves).

We consider two conditions for identifying melting from MAR. Specifically, we assume melting in MAR either when the daily-averaged integrated liquid water content (LWC) in the first meter of the snowpack exceeds 0.4% (equivalent to 0.4 mmwe in a 1 meter column) for at least three consecutive days or when total meltwater production over the day exceeds 0.4 mm w.e. The threshold value in the first condition (denoted as $LWC_{0.4}$) of 0.4% has been selected based on previous work comparing MAR outputs (version 3.2) and microwave melt estimates (Tedesco et al., 2007). The second condition is denoted as *MF0.4*. This less-restrictive condition is intended to capture both sporadic melt and melt which has percolated into the snowpack column below 1m.

2.2 Microwave satellite estimates of melt extent, duration

Spaceborne microwave satellites can detect the presence of melting over those regions where poor or no observations exist at high temporal resolution, because unlike sensors in the visible range, microwave sensors are weakly affected by the presence of clouds. In the case of active measurements (e.g., radar, scatterometer), the presence of wet snow is associated with a sharp decline in backscatter (σ^0) (Ashcraft and Long, 2000) where in the case of passive microwave data the detection is associated with an increase in brightness temperature (T_b) (Mote et al., 1993; Tedesco et al., 2007). In either passive or active microwave estimates, even the presence of a relatively small amount of liquid water (i.e. a few percent) triggers a substantial increase in the imaginary part of the dielectric constant (Ashcraft and Long, 2006; Ulaby and Stiles, 1980).

The Cryosphere Discuss., https://doi.org/10.5194/tc-2017-253
Manuscript under review for journal The Cryosphere
Discussion started: 22 December 2017
© Author(s) 2017. CC BY 4.0 License.

2.2.1 Active Microwave Data: QuikSCAT

We employ a wet snow high-resolution product described in Steiner and Tedesco (2014) to derive melt occurrence from active microwave data. Both melt occurrence and raw backscatter values used in this analysis use normalized backscattering values as measured by the Seawinds sensor onboard the QuikSCAT satellite at Ku band (13.4 GHz), with the enhanced resolution provided by the application of the Scatterometer Image Reconstruction (SIR) algorithm. (Long and Hicks, 2010). Both Ku- and C-band scatterometers have been used extensively to detect melt onset and freeze-up in Antarctica and Greenland (Drinkwater and Liu, 2000).

Threshold-based approaches with active microwave data, as used in this study, identify the point of melt onset based on the departure in σ^0 from values in dry-snow with various thresholds (Ashcraft and Long, 2000; Ashcraft and Long, 2006; Trusel et al., 2012). The approach used here derives melt occurrence from a threshold-based method (ft3), which identifies melt when backscatter falls 3 dB below the preceding winter mean (Steiner and Tedesco, 2014; Ashcraft and Long, 2006). This method, along with a wavelet approach have been evaluated over the AP with AWS data at 5 locations estimating melt occurrence from AWS as when 2m air temperature exceeded 0°C for more than 6 hours (Steiner and Tedesco, 2014).

In addition to the binary detection of melt, several methods have been proposed which relate seasonally-integrated backscatter reduction to measures for melt intensity (Wismann, 2000;Smith, 2003; Trusel et al., 2013). As these methods provide seasonally-cummulative values, we do not employ them in this study, although we do examine raw backscatter values as a proxy for melt flux.

2.2.2 Passive Microwave Data

We complement the assessment of MAR with estimates of melt extent and duration obtained from passive microwave observations which have been used in the past to assess melt occurrence in Antarctica and Greenland using brightness temperature from at 19.35 GHz with a horizontal polarization (Tedesco, 2007). One of the major disadvantages of passive microwave is the relatively coarse horizontal spatial resolution (25 km) with respect to the fine-scale topography characterizing the AP. However, the historical record for passive microwave data extends as far back as 1972. Threshold-based methods for melt detection from passive microwave data range from a combination of multiple frequencies and polarizations (Abdalati and Steffen, 1995) to using a single frequency, single polarization (e.g., Mote et al. 1993, Tedesco 2009), as is used in this study. Three algorithms are used here which are described in detail in (Tedesco, 2009). These include the *240*-algorithm where the threshold was determined as the value above which an increase in liquid water content above 1% no longer produces an increase in T_b, based on output of an electromagnetic model. The original threshold of 245K was found to be insufficiently sensitive and reduced to 240K for this study (Tedesco, 2007) (M. Tedesco, personal communication). The second algorithm uses the winter mean threshold-based method ALA:

$$T_c = T_{winter} * \alpha + T_{wet_{snow}} * (1 - \alpha) \quad (1)$$

The Cryosphere Discuss., https://doi.org/10.5194/tc-2017-253
Manuscript under review for journal The Cryosphere
Discussion started: 22 December 2017
© Author(s) 2017. CC BY 4.0 License.

where T_{winter} is mean winter (JJA) brightness temperature (T_b), T_{wet_snow} is wet snow brightness temperature (equal to 273K) and α is the mixing coefficient (equal to 0.47). Ashcraft and Long (2006) here presume a wet layer of 4.7 cm and a Liquid Water Content of 1%. Finally, the third algorithm (zwa) is based on the winter mean threshold.

$$T_c = T_{winter} + \Delta T \quad (2)$$

whereΔT is a threshold value, in this case 30K (Zwally and Fiegles, 1994).

2.3 AWS measurements

We assess MAR simulation of the near-surface atmosphere using temperature and wind speed data collected by three automatic weather stations (AWS) on the AP (Fig 1). Data from the Larsen Ice Shelf station is obtained from the University of Wisconsin Madison (AMRC, SSEC, UW-Madison) at a 3-hourly temporal resolution. AWS data from two additional sites on the Larsen Ice Shelf (AWS14 and AWS15) are obtained from the Institute for Marine and Atmospheric Research at Utrecht University (IMAU) at an hourly resolution. These also include values for the surface energy budget (Kuipers Munneke et al., 2012). We note that the Larsen IS station (-67.00 °S, -61.60°W) and the AWS14 station (-67.00°S, -61.5°W) are co-located to the same MAR grid cell.

AWS values are temporally averaged to obtain mean daily values for the comparison with the MAR outputs. Metrics are computed for December-January-February (DJF, summer). We did not compute a seasonal average when more than 5 consecutive days of data were missing. The five-day period was chosen as an upper limit for the length of a synoptic event, corresponding spatially to approximately 145 MAR grid cells (or half the model domain) of continuous flow in a single direction for an average windspeed of 3.4 m/s, i.e. the expected value for Larsen IS AWS station in DJF from 1999-2014 (Fig. 5c). Near-surface (2m) air temperature values are corrected for a difference between AWS station elevation and the elevation averaged by the corresponding MAR gridcell by calculating the elevation gradient from surrounding MAR gridcells and interpolating the final value for the AWS location's recorded elevation using the bedmap2 DEM (Fretwell et al., 2013). Differences in elevation values between MAR at the 10km resolution and those recorded at AWS stations were as large as 23 m. Maximum daily 2m air temperature (MaxT2m) is calculated as well because this measure may better indicate sporadic melt than values averaged to the daily scale. MaxT2m temperatures are extracted from available 3-hourly values and are used only when no more than one 3-hour measurement is missing during the day. Pressure values from AWS stations are also estimated at a approximately 2m above the surface, and compared to MAR values at the first atmospheric layer in MAR. Because the height of this layer is generally between 2 and 3 m above the surface, this is treated as an acceptable proxy for 2m pressure values. Pressure values from MAR are corrected for elevation using the hypsometric equation (Wallace and Hobbs, 1977).

2.4 Statistical Methods

To evaluate and quantify the agreement between MAR outputs and AWS data for temperature and wind speed we use a mean bias. Additional statistical measures used in supplemental data include the coefficient of determination (R^2), root mean squared error (RMSE) and mean error (ME) (Wilks, 1995). Also included in supplemental data, we

The Cryosphere Discuss., https://doi.org/10.5194/tc-2017-253
Manuscript under review for journal The Cryosphere
Discussion started: 22 December 2017
© Author(s) 2017. CC BY 4.0 License.

assess the extent to which each station is representative of larger scale climate variability by constructing correlation (R^2) maps between MAR values co-located with AWS stations vs all other gridpoints in the full MAR domain. We ignore all R^2 statistics where the p-value (indicating the probability that the underlying R value would exceed the result reported) exceeds 0.05.

To capture wind speed frequency distributions, we fit available data for each season for MAR (for the full 2000-2009 period), AWS (when AWS data is available) and MAR-R (MAR values collected only when AWS data is available) with a Weibull distribution. The shape (β) parameter roughly captures the degree of skew, with higher values being closer to an even normal distribution. The scale (λ) parameter approximates the peak frequency (we note that this is not equivalent to the mean). We report expected values for each windspeed distribution using the best Weibull fit.

3. Results: Melt Occurrence and Meltwater Production

In this section, we compare melt occurrence estimated by MAR with estimates from three passive microwave algorithms as well as QuikSCAT ft3 over the Antarctic Peninsula. We first identify spatial biases for melt occurrence at the domain scale, finding substantial differences in the center of the Larsen C Ice Shelf (the "CL" region, where PMW melt occurrence is highest) as well as to the north and west of the NE basin, a region which includes the former Larsens A and B ice shelves as well as the northernmost portions of the Larsen C ice shelf (the "NL" region, where MAR and QuikSCAT ft3 melt occurrence is highest) (Sect. 3.1). These differences could result from either weaknesses in the MAR representation of wind dynamics (discussed in Sect. 4) or from limitations of the satellite sensor or algorithm. Additionally, we compare climatology and inter-annual variability of melt extent (calculated by multiple algorithms) over the CL and NL region (Sect. 3.2).

3.1 Melt occurrence over the AP

Fig. 2 shows average annual melt occurrence (in days) over the model domain, estimated from the satellite-based algorithms QuikSCAT ft3 (Sect. 2.2.1) and three passive microwave algorithms (Sect. 2.2.2) as well as two metrics for melt derived from MAR outputs (Sect. 2.1). Because the MAR $MF_{0.4}$ melt metric shows more sensitivity to melt occurrence than the $LWC_{0.4}$ metric, it is used for comparison to QuikSCAT ft3 and PMW zwa (the most sensitive satellite-based algorithms). We use the term "PMWAll" to define the condition when all PMW algorithms report melt occurrence. Our primary focus is on the NE basin in the AP (shown in Fig. 1)

QuikSCAT ft3 generally estimates higher average yearly melt occurrence than either of the MAR melt metrics over the full domain. In the NE basin, the difference is on the order of 25 more days than the MAR $MF_{0.4}$ melt metric (Fig. 2f). Differences between QuikSCAT ft3 and $MF_{0.4}$ also show a strong latitudinal dependence in the NE basin, shifting from near agreement in the northern regions of the Larsen C Ice Shelf to QuikSCAT ft3 reporting over 500% of the melt days reported by MAR towards the southern edge. Melt onset is on the order of 22 days earlier in QuikSCAT ft3 than in $MF_{0.4}$ in the NE basin, except at the northern edge of the Larsen C ice shelf, where $MF_{0.4}$ reports average yearly melt onset as much as 25 days earlier than QuikSCAT ft3 (Supplemental Fig. 2).

The Cryosphere Discuss., https://doi.org/10.5194/tc-2017-253
Manuscript under review for journal The Cryosphere
Discussion started: 22 December 2017
© Author(s) 2017. CC BY 4.0 License.

A comparison between the two MAR melt metrics shows that $MF_{0.4}$ reports as much as 40 more days of melt than $LWC_{0.4}$ at the northern tip of the Larsen C Ice Shelf (Fig 2b vs Fig 2a). The portion of the Larsen C ice shelf which experiences an average of 25 days of melt or more extends as far south as 80.0°S on the eastern side of the Larsen C ice shelf according to the $MF_{0.4}$ metric but extends only to 70.50°S according to $LWC_{0.4}$. Towards the very south of the Larsen C Ice Shelf, the two MAR metrics show similar values, although $LWC_{0.4}$ reports melt onset as late as early January (Supplemental Fig. 2a) while $MF_{0.4}$ reports melt onset in December (Supplemental Fig 2b). The formulation for the $MF_{0.4}$ metric (considering melt at any time of the day for the full depth of the snowpack) suggests that the early season melt observed only by $MF_{0.4}$ is either sporadic (i.e. can refreeze, even immediately) and/or percolates below 1m in the snowpack in the south of the Larsen C Ice Shelf, i.e. below the depth range at which $LWC_{0.4}$ is calculated. Whereas QuikSCAT ft3 and MAR melt metrics report maximum melt occurrence in the north and west of the Larsen C Ice Shelf ($MF_{0.4}$ reporting > 60 days, Fig. 2b), PMW algorithms report maximum melt occurrence in the center-east of the Larsen C Ice Shelf, specifically 43 days (240, Fig. 2c), 57 days (ALA, Fig. 2d) and 69 days (zwa, Fig. 2e).

In summary, a comparison between observed and modeled data sources show two distinct spatial patterns for maximum melt occurrence. QuikSCAT ft3 as well as both MAR melt metrics show the highest range of melt days in the northern and western edges of the Larsen C Ice Shelf (including both high and low elevation regions) while PMW algorithms show the highest number of melt days in the center of the Larsen C Ice Shelf, where elevations are lower and topography is less complex. We hypothesize that the major difference in spatial patterns between algorithms/melt metrics are primarily related to the different resolutions of the data sources ad secondarily to the depths presumed for the calculation of meltwater content. This is true for both the MAR metrics and for the three PMW algorithms; the “ALA” algorithm, for example, presumes a 4.7cm depth and a 1% liquid water content. (see Sect. 2). To confirm this, we find the maximum depth to which meltwater percolates (according to MAR) associated with the number of days when melt occurs (according to PMW algorithms). Histograms for total PMW melt days in Supplemental Fig. 3 show three peaks (two major inflection points) for each algorithm which are used to create three classes for meltwater occurrence (“low”, “medium” and “high”). For these classes, the maximum depth to which meltwater percolates (in MAR) is shown in Supplemental Fig. 5 and the associated elevation and MAR meltwater production is shown in Supplemental Table 1.

Spatial regions defined as having “low” melt occurrence are highly heterogeneous. Bedmap2 (Fretwell et al., 2013) reports a large range of elevations while MAR reports low coincident meltwater production and a relatively shallow meltwater depth. Both the ALA and zwa algorithms report melt at higher elevations (above approximately 1300m and 1900m, respectively) than the 240 algorithm, which neither reports any melt occurrence above 1100m in the NE basin nor at lower elevations to the north and south. (Supplemental Material Table 1, rows 1,4,7 and Fig. 5). Where melt occurrence is low, the 240 and ALA algorithms generally detect melt only where MAR reports a maximum meltwater percolation depth below 0.4 m, (Supplemental Fig 5a,b), whereas the zwa algorithm can detect melt at a substantially shallower depth of 0.1 m (Supplemental Fig 5c). Although generally meltwater in MAR rarely percolates below 3m, in low melt-occurrence regions, modeled meltwater occasionally percolates below 10m in the beginning of the melt season (Supplemental Fig. 5 a,b,c, N column). We remind the

The Cryosphere Discuss., https://doi.org/10.5194/tc-2017-253
Manuscript under review for journal The Cryosphere
Discussion started: 22 December 2017
© Author(s) 2017. CC BY 4.0 License.

reader that melt occurrence within the firn layer (as calculated by MAR $MF_{0.4}$) will capture melt that can refreeze immediately, so this does not necessarily correspond to melt which is retained in the snowpack. Rather, the snowpack layer depth represents the deepest layer which is affected by the melt process according to MAR.

By contrast, in high PMW melt occurrence regions in the NE basin, MAR consistently reports high coincident meltwater production, low elevations and the deepest average meltwater percolation in the region. In the month of January, we find that where PMW algorithms report melt, coincident MAR meltwater percolates to 2 meters into the snowpack for 35-47% of the total day-pixels in the NE basin which report any melt, and as deep as 3 meters for more than 30% of total day-pixels (Supplemental Table 1, 240-H, ALA-H, zwa-H, Fig 5 g,h,i).

To quantify the two major spatial trends for maximum melt occurrence, i.e. (a) PMW in the center-east of the Larsen C ice shelf and (b) QuikSCAT ft3 and MAR in the northwest of the NE basin, we (a) explicitly calculate concurrent melt occurrence in all PMW algorithms (PMWAll) for the first region and (b) define the latter geographically in order to include most of the Northern NE basin, but deliberately exclude center-east of the Larsen C ice shelf region where PMW melt is highest. The first region "CL" (Center Larsen), where all PMW algorithms agree on high melt occurrence, is defined where PMWAll reports average yearly total melt days exceeding one standard deviation from the mean for the NE basin. Mean elevation for the CL region is 42.70±17.70σ m (where σ is one standard deviation) . PMWAll reports a mean annual 36 days of melt occurrence (vs 21 days derived from $MF_{0.4}$) and a mean PMWAll-coincident annual MAR meltwater production of 96 mmwe/100km^2 (vs 143 mmwe/100km^2 when $MF_{0.4}$ reports melt)(Supplemental Table 1, row 11,12).

The "NL" (Northern Larsen) mask is defined by finding the mean latitude of the CL region and including all portions of the NE basin above this latitude, but excluding the CL region (Fig. 4c, inset). In the NL region, elevation is highly-variable, with a mean value ~600m and MAR and QS detect melt both earlier and more often than for PMW algorithms. Both masks are shown in the inset in Fig. 3a and Fig. 4c and are used for subsequent analysis of inter-annual meltwater production in MAR.

3.2 Climatology and inter-annual trends for melt extent at the sub-basin scale

We compare the seasonal cycle and interannual variability of melt as modeled by MAR vs observations for both the CL and NL regions by computing regional melt extent over the period (total melt extent area for each day in NDJF), both yearly and as a climatological average. The PMWAll algorithm is typically treated as the most restrictive condition while the PMW zwa and QuikSCAT ft3 are the most sensitive. Melt extent is defined as the total area reporting melt daily between Nov 1st and February 28th (austral summer, including November to show early melt)(Fig. 3).

The melt extent climatology for PMWAll in the CL region shows an early pulse of melt around Dec 15th with melt extent peaking in January, followed by a series of increasingly smaller melt pulses ending with refreeze at the end of February. While MAR shows peak melt extent at the same point in the season, the progression from melt onset is more gradual, average peak melt extent is generally smaller and interannual variability (indicated by the grey envelope) during peak melt extent is larger (Fig. 3c vs Fig. 3a). In the CL region, the PMWAll metric is generally restricted by the low sensitivity of the 240 algorithm. Interannual variability for melt extent is substantial,

The Cryosphere Discuss., https://doi.org/10.5194/tc-2017-253
Manuscript under review for journal The Cryosphere
Discussion started: 22 December 2017
© Author(s) 2017. CC BY 4.0 License.

with PMWAll reporting a larger melt extent than MAR towards the middle of the melt season in most years (Fig. 3b,d), but not necessarily during melt onset or its ending. In the CL region, PMWAll reports a larger melt extent throughout the melt season during 2000-2001 and 2001-2002 (Fig. 3d). During three periods, MAR reports a larger melt extent than PMWAll, including 1999-2000, the latter half of the 2002-2003 season and the 2003-2004 season. While the highly-sensitive PMW zwa algorithm (Fig. 3e,f) reports sporadic periods where MAR melt extent is larger (during the 1999-2000 and 2003-2004 melt seasons, for example), zwa generally reports either a larger melt extent or general agreement with MAR. Similarly, melt extent derived from the QuikSCAT ft3 algorithm consistently shows a larger melt extent than MAR, except for a few short periods towards the end of the season in 1999-2000 and 2003-2004 (Fig. 3 g,h). We note that for several years, both QuikSCAT ft3 and PMW zwa report substantial melt occurrence early in the season (~Nov 15th) and that the QuikSCAT ft3 climatology frequently reports melt occurrence in the CL region well after February (Fig 3g).

Note that the NL region includes areas which reported low melt occurrence in all PMW algorithms, variable meltwater percolation depth in MAR, and a large range of elevations (Sect 3.1), implying that the mask defined by the combined PMWAll algorithm is less clearly linked to specific modeled physical properties in this region. Here, the MAR melt extent climatology (Fig. 4a,b) is consistently larger than PMWAll throughout the season (Fig. 4c,d). In comparison to the zwa (Fig. 4c) and QuikSCAT ft3 (Fig. 4g) algorithms, MAR reports less melt extent in the middle of the season (with peak melt extent in January), but larger melt extent at the beginning and end of the melt season. As compared with the CL region, the MAR climatological melt extent shows less inter-annual variability (grey envelope, Fig. 4a). During the 2000-2001 and 2001-2002 melt seasons, MAR shows a larger melt extent than PMWAll (Fig. 4d), but less than the PMW zwa (Fig 4f) or QuikSCAT ft3 (Fig. 4h) algorithms. We find that during the 2005-2006 season, MAR shows greater melt extent than PMWAll, consistently less than QuikSCAT ft3, but reports a greater melt extent tha zwa only towards the end of the season. We consider the condition where only QuikSCAT ft3 or PMW zwa show a greater melt extent than MAR to likely be indicative of sporadic surface melt.

In summary, we conclude that in the CL region, MAR reports a larger melt extent during that period than PMWAll (which is highly-restrictive), but a smaller melt extent than either the PMW zwa or QuikSCAT ft3 algorithms, which are more sensitive. Notably, MAR melt occurrence is comparatively low during the peak melt period. By contrast, in the NL region, MAR reports greater melt occurrence than the most restrictive measure (PMWAll) during peak melt, but far less than the highly-sensitive QuikSCAT ft3 algorithm. The interannual comparison suggests that MAR shows substantially less melt occurrence than observations during the 2000-2001 and 2001-2002 seasons in the CL region, but not the NL region.

4. Results: Wind and Temperature Biases at the Larsen Ice Shelf station

The East AP is substantially colder than the West AP, and temperature-driven melt primarily results from either warm northerly flow from lower latitudes or from westerly föhn flow over the spine of the AP. Here, we assess the bias in temperature and melt occurrence associated with wind direction at three AWS stations located on the Larsen C Ice Shelf (shown in Fig. 1). We first discuss wind direction and wind speed biases during the summer season at all

The Cryosphere Discuss., https://doi.org/10.5194/tc-2017-253
Manuscript under review for journal The Cryosphere
Discussion started: 22 December 2017
© Author(s) 2017. CC BY 4.0 License.

three locations (without regard to melt occurrence) (Sect. 4.1). We then find temperature/wind direction biases specifically associated with melt occurrence in MAR, PMWAll and QuikSCAT ft3, in order to capture which wind direction/temperature biases lead to a disproportionate amount of observed melt which is not captured by MAR (Sect. 4.2). All MAR and satellite data used are co-located to the grid cell associated with the AWS station (Fig. 1), and we remind the reader that all three stations, at the eastern edge of the CL region (Fig. 2 inset), are located where MAR reported substantially less melt occurrence than PMW algorithms or QuikSCAT ft3.

4.1 Aggregate wind direction biases

Fig. 5 shows wind frequency distributions during the summer season (AWS, MAR-R, MAR from left to right columns, Larsen IS station, AWS 14 and AWS 15 from top to bottom), color-coded for wind direction as represented by the pie graph at the top. We note that AWS data uses 3-hourly data for wind speed and direction without daily-averaging, while MAR produced daily-averaged outputs, For this reason, a direct comparison between Weibull parameters derived from MAR vs AWS data is not meaningful, although we show comparisons between different stations (for the same data source) .The Larsen IS station has full temporal coverage during the QuikSCAT period while AWS14 and AWS15 were installed after termination of the QuikSCAT mission. These last two stations are used in this study to demonstrate the consistency of wind biases at multiple locations, as well as how wind biases vary by latitude (AWS15 being located slightly to the south). Whereas MAR is dominated northerly winds at it's lower range of windspeeds (in yellow and blue), AWS data shows a greater frequency of southwesterly winds at the higher range of windspeeds (> 8 m/s). In general, even at lower wind speeds (2-5 m/s), AWS data shows more southwesterly winds than either MAR-R or MAR. This is especially relevant at the southern AWS15 station, where modeled temperature correlates with a larger region of the Larsen IS than temperatures modeled by MAR for the AWS14 station (Supplemental Fig. 6). Observed wind direction (without consideration for wind speed) at AWS15 shows more southwesterly flow (Fig. 5g) than either MAR-R or MAR (Fig. 5 h,i), which show a substantially higher percentage of southeasterly and northerly flow instead.

Specifically, while both MAR and AWS show a higher proportion of northerly (vs southerly) winds, the proportion of northerly winds in MAR is slightly higher (Table 1). While both MAR and AWS report a larger proportion of easterly (vs westerly) flow, MAR reports 64% of flow to be easterly where AWS reports only 55% easterly flow. We show that MAR melt occurrence at the Larsen Ice Shelf station is concurrent with both increased northerly and westerly flows. On days when MAR reports melt (compared to days with no melt), northerly winds are more frequent (according to both MAR and AWS estimates), and the proportion of westerly winds increases slightly in MAR but decreases slightly in AWS data (Table 1).

When daily-averaged temperature (AvgT2m) values are high, it is more likely that melt is sustained, while high maximum daily temperatures (MaxT2m) can also occur during sporadic melt. Melt occurrence is strongly influenced by the temperature of the snow column as well as at the surface; internal melting can occur even when the surface is frozen due to net outgoing longwave radiation (Holmgren 1971)(Hock 2005) In general, we find a small, but consistent warm MAR bias for AvgT2m, and a consistent cold MaxT2m bias. However, when we restrict the dataset to days when AWS 2m-temperature estimates exceed 0°C, (a condition where melt is most likely), MAR indicates a

The Cryosphere Discuss., https://doi.org/10.5194/tc-2017-253
Manuscript under review for journal The Cryosphere
Discussion started: 22 December 2017
© Author(s) 2017. CC BY 4.0 License.

cold bias for AvgT2m and an enhanced cold bias for MaxT2m, i.e. while MAR shows an overall warm bias, this bias is reversed at the temperature ranges where melt is likely (although melt is still possible due to other elements in the energy balance). On days when MAR meltwater production meets the $MF_{0.4}$ criteria, we find that the magnitude of all biases is greatly reduced. In particular, we note that the MaxT2m bias for westerly winds (for the ALL condition) is substantial, showing a -2.42°C cool bias in MAR for all available data and -3.04°C when data is restricted to days when MaxT2m > 0°C.

4.2 Wind and temperature biases concurrent with observed melt occurrence

Three wind direction biases are dominant on days when observed sources (either PMW All or QuikSCAT ft3) report melt, but MAR does not. We refer to the condition where PMWAll reports melt (but MAR does not) as "PMWEx" (i.e. PMW exclusive-or), with the equivalent condition for QuikSCAT ft3 called "QSEx". We focus on these specific wind biases and find the associated temperature biases. Supplemental tables 2-7 include R^2, RMSE and mean bias values for both surface pressure and daily AvgT2m at all three stations.

4.2.1 Observed northeasterly flow

The largest proportion of melt occurrence for either MAR, PMWEx or QSEx is reported when northeasterly winds are dominant, specifically when winds are recorded by the Larsen Ice Shelf AWS station as northeasterly (0°- 90°). Northeasterly AWS flow accounts for a large proportion of general flow and an even larger proportion of flow when either MAR or PMWEx report melt, i.e. 36% of general flow, 39% of days where MAR reports melt, 42% of days where PMWEx reports melt and 36% of days where QSEx reports melt. On days when AWS reports northeasterly winds, MAR primarily reports northeasterly flow (0°- 90°, case 1), but also reports a substantial bias for northwesterly flow (270°-360°, case 2). In case 2, associated temperature biases may be influenced by the inclusion of warmer westerly winds in MAR. We add that the majority of northeasterly AWS flow is actually captured in a narrower northeasterly band in MAR from 0-45°, accounting for 13.4% of ALL days. We examine these two cases separately to quantify how a modeled westerly wind bias affects temperature and melt (in comparison to the case when wind direction matches observed estimates). Supplemental tables 8-10 contain relative proportions of each case (flow bias) divided by the general melt restriction (i.e. MAR, QSEx or PMWEx), as well as the timeseries mean and biases for AvgT2m, AvgT2m>0°C (excluding days when AvgT2m values from AWS are below 0°C), MaxT2m and MaxT2m >0°C.

In the instance where northeasterly flow is modeled accurately (case 1, Fig. 6a), modeled temperature values are clustered around 0°C, whereas AWS-observed temperatures (especially when only satellite-observed melt occurs) are higher. When MAR reports melt, MAR AvgT2m values cluster near 0°C, with a small overall warm bias (0.69°C). Under omission conditions (PMWEx and QSEx), AvgT2m values are lower, and MAR bias is slightly cold, although standard deviation is high. As with all flow cases, only QuikSCAT ft3 shows melt at very low observed AvgT2m values. By contrast, AWS MaxT2m values are substantially higher than MAR values (the latter clustering around 0°C) (Fig. 6b). We find that where QuikSCAT ft3 uniquely reports melt (QSEx), AvgT2m values at the lower range of temperatures report a stronger cool MAR bias for MaxT2m .

The Cryosphere Discuss., https://doi.org/10.5194/tc-2017-253
Manuscript under review for journal The Cryosphere
Discussion started: 22 December 2017
© Author(s) 2017. CC BY 4.0 License.

In case 2, AvgT2m values show a small warm MAR bias in all melt conditions, i.e. for ALL data points (0.79°C), for when MAR shows melt (0.82°C), and finally for both the PMWEx (0.44°C) and QSEx(0.65°C) conditions (Supplemental Table 8). However, when MAR reports melt and AWS AvgT2m values exceed 0°C, there is a substantial cold bias (-1.13°C)(Fig 6c), which may lead to reduced meltwater production. In contrast to case 1, modeled MaxT2m values in case 2 do not cluster around 0°C (Fig. 6b,d) and MAR melt days report larger MaxT2m values.

In summary, when MAR reports westerly flow, Avg T_s values are higher (as is melt occurrence). As with the comparison with case 1 and case 2, we find that in all instances when MAR reports northeasterly flow (with all AWS-observed wind directions considered), AvgT2m and MaxT2m temperatures cluster near 0°C (Fig. 6e,f), whereas when MAR reports northwesterly flow (with all AWS wind directions taken into consideration), MaxT2m values are, on average, higher, and the temperature bias is narrowed (Fig. 6 g,h). Expected values for windspeeds for each condition based on a Weibull fit show comparable expected values, but larger standard deviations for AWS-estimated windspeeds when MAR reports northwesterly flow (Fig. 6 c,d g,h).

4.2.2 Observed southwesterly flow

For all days in the summer season ("ALL", i.e. without regard for melt occurrence), we find that MAR reports 15% of winds to be southwesterly at the Larsen Ice Shelf station location while AWS reports ~ 30% southwesterly flow. We note that the relative proportions of southwesterly/southeasterly flow in AWS is approximately reversed in MAR, with AWS reporting 18.3% of flow to be southwesterly and MAR reporting 29.2% southwesterly flow. We focus specifically on the condition where both MAR and AWS report southwesterly flow (between 180° and 270°), which accounts for 5.7% of total flow and only 4.9% of MAR melt days, but a larger proportion of days where only observed sources report melt, i.e. 5.6% for the PMWEx condition and 8% for the QSEx condition.

As with case 2 for northwesterly winds in section 4.2.1, MAR captures higher AvgT2m values which frequently exceed 0°C, with a slight cool MAR bias when AvgT2m > 0°C (Fig 7a). The PMWEx and QSEx conditions report melt at lower temperature values, where the MAR bias is slightly warmer. Although a cold MAR bias persists, MaxT2m values are, in general, higher with AWS and MAR values showing greater agreement (Fig 7b). Expected windspeeds for southwesterly winds are substantially higher (with a greater standard deviation) than the base condition when wind direction is not considered, with AWS reporting an even higher standard deviation (i.e. high-speed sporadic winds).

5. Discussion and Conclusions

In the aggregate, we conclude that MAR shows lower melt occurrence than satellite estimates in the center and east of the Larsen C ice shelf (i.e. the CL region, where eastward föhn flow is likely limited in MAR), while in the north and west of the NE basin (i.e. the NL region which is most immediately affected by föhn flow), MAR reports melt occurrence largely concurrent with satellite estimates. For example, within the CL region, there are periods during the 2001-2002 season when MAR reports no meltwater production, but raw QuikSCAT backscatter values report periods where over 300 km^2 of surface area show backscatter values dipping below -15 dB (Supplemental Fig.

The Cryosphere Discuss., https://doi.org/10.5194/tc-2017-253
Manuscript under review for journal The Cryosphere
Discussion started: 22 December 2017
© Author(s) 2017. CC BY 4.0 License.

8e).We remind the reader that raw backscatter values from QuikSCAT have previously been used to estimates melt flux over the AP (Trusel et al., 2013; Trusel et al., 2012).

In comparison to AWS estimates, MAR displays a general warm bias in the East AP at lower temperatures where melt is less likely to occur, but which may still impact the refreeze process. However, when maximum daily temperatures (MaxT2m) and average daily temperatures (AvgT2m) exceed 0°C, MAR shows a substantial cold bias which may limit melting. We note a smaller proportion of westerly winds in MAR compared to observed values at the Larsen Ice Shelf AWS station, especially an absence of southwesterly flow, which tends to have higher observed windspeeds. The general cold bias in MAR is partially closed when observed northeasterly winds are reported by MAR as northwesterly, i.e. MAR reports both higher AvgT2m and MaxT2m values as well as greater melt occurrence. Similar biases are shown for southwesterly flow, which accounts for a disproportionate amount of satellite-observed melt which is not captured by MAR. The importance of westerly winds is demonstrated during mid-December in the 2001-2002 season, at which point satellite-based melt extent in the CL region increases substantially, while MAR melt extent declines (Supplemental Fig. 8a). This period is concurrent with an increase in westerly winds at the Larsen IS AWS station which are not modeled MAR (Supplemental Fig 9b vs f). Additionally, we note that shortly after this point, AWS AvgT2m temperatures consistently exceed MAR AvgT2m values until the end of the season (Supplementary Fig. 10).

Previous work has suggested that southwesterly föhn winds can result from gap flow (Elvidge et al. 2015), although we note that the southwesterly jets studied in this single campaign were typically cooler and moister than surrounding air (i.e. föhn flow produced from isentropic drawdown). We note that the low windspeed bias in MAR may have a minor impact overall, but could strongly impact melt in the East AP if southwesterly flow is more accurately captured in future versions of MAR. We hypothesize that the underestimation of westerly flow at the eastern reaches of the Larsen C ice shelf is likely due to the hydrostatic assumption (allowing for no vertical acceleration of air mass) preventing eastward, downward flow in the near-surface atmosphere. The implementation of a non-hydrostatic model will likely be required to fully capture föhn flow in the East AP (Hubert Gallée, personal communication). We conclude that the relative absence of fast, warm westerly and southwesterly winds contributes to a lack of MAR melt in the CL region as compared to satellite estimates.

Previous literature has pointed to several limitations in the remote sensing data sources used here which are either intrinsic to the satellite data itself or a product of the algorithm selected for melt detection. Products derived from QuikSCAT are limited in temporal resolution because the satellite passes at a twice-daily scale, and may therefore ignore sporadic melt occurring at other times of day. However, previous studies have compared total melt days from the QuikSCAT ft3 algorithm with a measure derived from surface temperature at seven automatic weather stations and shown a positive QuikSCAT ft3 bias compared to AWS (Steiner and Tedesco, 2014). Similarly, all PMW algorithms are limited by a relatively low resolution (25km) and twice-daily passes. Periods of melt occurrence have also been shown to be highly sensitive to the choice of algorithm (Tedesco 2009). Because of the high topographic variability of the NL region (especially near the spine of the AP), it is possible that PMW algorithms are under-reporting melt occurrence due to low horizontal spatial resolution. A higher-resolution passive microwave product may better resolve this issue.

© Author(s) 2017. CC BY 4.0 License.

In the northernmost portions of the NL region, sporadic MAR-modeled meltwater percolates deeply into the snowpack in November (as deep as 10m early in the season in some years), which is consistent with MAR $MF_{0.4}$, PMW zwa and QuikSCAT ft3 reporting melt occurrence at this point while other algorithms/melt metrics do not. The deep percolation of meltwater is potentially enabled by low density snow early in the season. This early-season melt is frequently followed by a near-complete refreeze. Future work will focus on the interannual variability of early-season melt as this may have a substantial impact on the density of the firn layer in the Larsen C ice shelf.

In light of the biases reviewed here, we report MAR meltwater production over the 1999-2009 period (Fig. 8) and consider the potential implications of the wind/temperature biases found in this analysis on regional meltwater production. Over the full study domain, the total annual meltwater production estimated by MAR shows substantial inter-annual variation with the NE basin accounting for the highest aggregate meltwater production, closely followed by the SW basin (in green). The NE basin is divided into three regions: the NL and CL masks and the remainder of the basin. We note that the SW basin does not covary with the NE basin (with all subregions taken together) and the subregions of the NE basin do not consistently covary with one another. The meltwater production shown here does not account for refreeze and we note that the effects of refrozen melt on the snowpack will vary regionally depending on local properties. The NL region dominates meltwater production in the NE basin in most years except for 1999-2000, 2002-2003 and 2003-2004. The 2001-2002 melt season shows the second lowest overall melt production during the study period (only the preceding year is lower). Declining aggregate meltwater production across the AP does not necessarily correspond to declining meltwater production in the most vulnerable regions of the northeastern AP (including the Larsen C ice shelf). Because melt in the NL region is particularly sensitive to föhn-induced melt, we note that changes in circulation patterns may affect the northwest regions differently than the southern regions. The strong relationship between wind direction and temperature bias points to the need for isolating dominant inter-annual patterns of melt in the Northern Larsen C Ice Shelf and associating them with large-scale atmospheric drivers.

References

Abdalati, W., and Steffen K.: Passive Microwave-Derived Snow Melt Regions on the Greenland Ice Sheet, Geophysical Research Letters., 22 (7), 787–790, doi:10.1029/95GL00433, 1995.

Ahrens, C. Donald.: Meteorology Today : An Introduction to Weather, Climate, and the Environment. Eighth edition. Thomson/Brooks/Cole, Belmont, CA, 2007.

Amory, C., Trouvilliez, A., Gallée, H., Favier, V., Naaim-Bouvet, F., Genthon, C., Agosta, C., Piard, L., and Bellot. H.: Comparison between Observed and Simulated Aeolian Snow Mass Fluxes in Adélie Land, East Antarctica., The Cryosphere 9 (4), 1373–83, doi:10.5194/tc-9-1373-2015, 2015.

Ashcraft, I. S., and Long. D.G.: SeaWinds Views Greenland: In Geoscience and Remote Sensing Symposium, 2000. Proceedings. IGARSS 2000. IEEE 2000 International, 3,1131–1133, 2000.

© Author(s) 2017. CC BY 4.0 License.

Ashcraft, I. S., and Long. D.G.: Comparison of Methods for Melt Detection over Greenland Using Active and Passive Microwave Measurements, International Journal of Remote Sensing, 27 (12), 2469–88, doi:10.1080/01431160500534465, 2006.

Barrand, N. E., Vaughan, D. G., Steiner, N., Tedesco, M., Kuipers-Munneke, P. , Van den Broeke, M. R., and Hosking, J. S.: Trends in Antarctic Peninsula Surface Melting Conditions from Observations and Regional Climate Modeling, Journal of Geophysical Research: Earth Surface, 118 (1), 315–330, doi:10.1029/2012JF002559, 2013.

Bell, R, E., Chu, W. Kingslake, J., Das, I., Tedesco, M., Tinto, K.J., Zappa, C.J., Frezzotti, M., Boghosian, A., and Lee.W.S.: Antarctic Ice Shelf Potentially Stabilized by Export of Meltwater in Surface River, Nature, 544 (7650), 344–348. doi:10.1038/nature22048, 2017.

Beran, D.W..: Large Amplitude Lee Waves and Chinook Winds, Journal of Applied Meteorology, 6 (5),865–877. doi:10.1175/1520-0450(1967)006<0865:LALWAC>2.0.CO;2., 1967.

Braithwaite, R. J.: On Glacier Energy Balance, Ablation, and Air Temperature, Journal of Glaciology, 27, 381–91, 1981

Brandt, R. E., and Warren, S.G..: Solar-Heating Rates and Temperature Profiles in Antarctic Snow and Ice, Journal of Glaciology, 39, 99–110. doi:10.1017/S0022143000015756, 1993.

Brun, E, David, P., Sudul, M. and G Brunot, G.: A Numerical Model to Simulate Snow-Cover Stratigraphy for Operational Avalanche Forecasting, Journal of Glaciology, 38,13–22, 1992.

Cape, M. R., Vernet, M., Skvarca, P., Marinsek, S., Scambos, T. and Domack, E.: Foehn Winds Link Climate-Driven Warming to Ice Shelf Evolution in Antarctica. Journal of Geophysical Research: Atmospheres, 120 (21) 11, 37-11, doi:10.1002/2015JD023465, 2015.

De Ridder, K., and Gallée, H.: Land Surface-Induced Regional Climate Change in Southern Israel, Journal of Applied Meteorology, 37 (11), 1470–1485, 1998.

Dee, D. P., Uppala, S. M., Simmons, A. J., Berrisford, P., Poli, P., Kobayashi, S., Andrae, U. et al., The ERA-Interim Reanalysis: Configuration and Performance of the Data Assimilation System, Quarterly Journal of the Royal Meteorological Society, 137 (656), 553–597, doi:10.1002/qj.828, 2011.

© Author(s) 2017. CC BY 4.0 License.

Drinkwater, M.R., and Liu, X.: Seasonal to Interannual Variability in Antarctic Sea-Ice Surface Melt, IEEE Transactions on Geoscience and Remote Sensing, 38(4), 1827–1842, doi:10.1109/36.851767, 2000.

Dutra, E., Sandu, I., Balsamo, G., Beljaars, A., Freville, H., Vignon, E., and Brun. E.: Understanding the ECMWF Winter Surface Temperature Biases over Antarctica, Technical Memorandum, 762, 2015.

Elvidge, A. D., Renfrew, I.A., King, J.C., Orr, A., Lachlan-Cope, T.A., Weeks, M. and Gray, S.L.: Foehn Jets over the Larsen C Ice Shelf, Antarctica, Quarterly Journal of the Ro/yal Meteorological Society, 141(688), 698–713. doi:10.1002/qj.2382., 2015.

Fettweis, X., Franco, B., Tedesco, M., van Angelen, J.H., Lenaerts, J. T. M., Van den Broeke, M. R. and Gallée, H.: Estimating the Greenland Ice Sheet Surface Mass Balance Contribution to Future Sea Level Rise Using the Regional Atmospheric Climate Model MAR, The Cryosphere 7 (2), 469–489, doi:10.5194/tc-7-469-2013, 2013.

Fettweis, X, Gallée, H., Lefebre, F., and Van Ypersele. J., Greenland Surface Mass Balance Simulated by a Regional Climate Model and Comparison with Satellite-Derived Data in 1990–1991, Climate Dynamics 24 (6), 623–640, 2005.

Fettweis, X., Box, J.E., Agosta, C., Amory, C., Kittel, C., and Gallée, H.: Reconstructions of the 1900-2015 Greenland Ice Sheet Surface Mass Balance Using the Regional Climate MAR Model, The Cryosphere Discussions, November, 1–32, doi:10.5194/tc-2016-268, 2015.

Franco, B., Fettweis, X., Lang, C., and Erpicum, M.: Impact of Spatial Resolution on the Modelling of the Greenland Ice Sheet Surface Mass Balance between1990–2010, Using the Regional Climate Model MAR, The Cryosphere 6 (3), 695–711. doi:10.5194/tc-6-695-2012, 2012.

Fretwell, P., Pritchard, H. D., Vaughan, D. G., Bamber, J. L., Barrand, N. E., Bell, R., Bianchi, C. et al.: Bedmap2: Improved Ice Bed, Surface and Thickness Datasets for Antarctica, The Cryosphere, 7 (1), 375–393, doi:10.5194/tc-7-375-2013, 2013.

Gallée, H., and Schayes.G.: Development of a Three-Dimensional Meso-Gamma Primitive Equation Model: Katabatic Winds Simulation in the Area of Terra Nova Bay, Antarctica, Belgian Science Policy Office, 1994.

Gallée, H., Trouvilliez, A., Agosta, C., Genthon, C., Favier, V., and Naaim-Bouvet, F.: Transport of Snow by the Wind: A Comparison Between Observations in Adélie Land, Antarctica, and Simulations Made with the Regional Climate Model MAR, Boundary-Layer Meteor., 146 (1), 133–47, doi:10.1007/s10546-012-9764-z, 2013.

© Author(s) 2017. CC BY 4.0 License.

Gilbert, R. O.: Statistical Methods for Environmental Pollution Monitoring, Van Nostrand Reinhold Co., New York, NY, 1987.

Glasser, N. F., and Ted A. Scambos.: A Structural Glaciological Analysis of the 2002 Larsen B Ice-Shelf Collapse., J. of Glaciology 54 (184):3–16, 2008

Grosvenor, D. P., King, J.C., Choularton, T. W., and Lachlan-Cope, T.: Downslope Föhn Winds over the Antarctic Peninsula and Their Effect on the Larsen Ice Shelves. Atmos. Chem. and Phys., 14 (18), 9481–9509., https://doi.org/10.5194/acp-14-9481-2014., 2014.

Hock, R.: Glacier Melt: A Review of Processes and Their Modelling, Progress in Phys .Geog., 29 (3), 362–91, doi:10.1191/0309133305pp453ra., 2005.

Holland, P.R., Hugh F. J. Corr, H. D. Pritchard, Vaughan, D.G., Arthern, R.J., Jenkins, A., and Tedesco, M.: The Air Content of Larsen Ice Shelf, Geoph. Res. Let., 38 (10), doi:10.1029/2011GL047245, 2011.

Holmgren, B.: *C*limate and Energy Exchange on a Sub-Polar Ice Cap in Summer: Arctic Institute of North America Devon Island Expedition 1961-1963. Acta Univ. Upsal. Abstracts of Uppsala Diss. from the Faculty of Science, pt. 3. Meteorologiska Institutionen Uppsala Universitet., 1971.

Holton, J.: The General Circulation, in: An Introduction to Dynamic Meteorology, 4th ed., Elsevier Inc., 329–337, 2004.

Hubbard, B., Luckman, A., Ashmore, D.W., Bevan, S., Kulessa, B., Kuipers-Munneke, P., Philippe, M. et al.: Massive Subsurface Ice Formed by Refreezing of Ice-Shelf Melt Ponds, Nat. Comm., 7 (June), 11897., doi:10.1038/ncomms11897, 2016.

Jansen, D., Kulessa, B., Sammonds, P. R., Luckman, A., King, E. C. and Glasser, N.F.: Present Stability of the Larsen C Ice Shelf, Antarctic Peninsula, J. of Glac., 56 (198), 593–600, 2010.

Kingslake, J., Ely, J.C., Das, I., and Bell, R.E.: Widespread Movement of Meltwater onto and across Antarctic Ice Shelves, Nature, 544 (7650), 349–352, doi:10.1038/nature22049, 2017.

Koh, G., and Jordan, R.: Sub-Surface Melting in a Seasonal Snow Cover. J. of Glaciology, 41 (139): 474–482. doi:10.3189/S002214300003481X, 1995.

© Author(s) 2017. CC BY 4.0 License.

Kuipers-Munneke, P., van den Broeke, M. R., King, J. C., Gray, T., and Reijmer, C. H.: Near-Surface Climate and Surface Energy Budget of Larsen C Ice Shelf, Antarctic Peninsula, The Cryosphere, 6 (2), 353–363, doi:10.5194/tc-6-353-2012, 2012.

Kuipers Munneke, P., Picard, G., van den Broeke, M. R., Lenaerts, J. T. M., and van Meijgaard, E.: Insignificant Change in Antarctic Snowmelt Volume since 1979: Antarctic Snowmelt Volume, Geoph. Res. Lett., 39(1), doi:10.1029/2011GL050207, 2012

Kuipers-Munneke, P., Ligtenberg, S.R.M., Van Den Broeke, M.R., andVaughan, D.G.: Firn Air Depletion as a Precursor of Antarctic Ice-Shelf Collapse, J. of Glaciology 60 (220), 205–14, doi:10.3189/2014JoG13J183, 2014.

Lenaerts, J. T. M., Lhermitte, S., Drews, R., Ligtenberg, S. R. M., Berger, S., Helm, V., Smeets, C. J. P. P. et al.: Meltwater Produced by Wind–albedo Interaction Stored in an East Antarctic Ice Shelf, Nat. Clim. Change, 7 (1), 58–62, doi:10.1038/nclimate3180, 2016.

Liston, G.E., Bruland, O.,Winther, J., Elvehøy, H. and Sand, K.: Meltwater Production in Antarctic Blue-Ice Areas: Sensitivity to Changes in Atmospheric Forcing, Polar Research, 18 (2), 283–290, doi:10.3402/polar.v18i2.6586, 1999a.

Liston, G. E., Winther, J., Bruland, O., Elvehøy, H. and Sand, K.: Below-Surface Ice Melt on the Coastal Antarctic Ice Sheet, J. of Glaciology 45 (150): 273–85. doi:10.3189/S0022143000001775, 1999b.

Liu, H., Wang, L., and Jezek, K.C.: Spatiotemporal Variations of Snowmelt in Antarctica Derived from Satellite ScanningMultichannel Microwave Radiometer and Special Sensor Microwave Imager Data (1978–2004), J. of Geoph. Res.: Earth Surface, 111 (F1), doi:10.1029/2005JF000318, 2006.

Long, D.G., and Hicks, B.R.: Standard BYU QuikSCAT/SeaWinds Land/Ice Image Products, QuikScat Image Product Documentation, Brigham Young Univ., Provo, UT, 2000.

Luckman, A., Elvidge, A., Jansen, D., Kulessa, B., Kuipers-Munneke, P., King, J., and Barrand, N.E., Surface Melt and Ponding on Larsen C Ice Shelf and the Impact of Föhn Winds, Antarctic Science, 26 (6), 625–635, doi:10.1017/S0954102014000339, 2014.

MacAyeal, D.R., and Sergienko O.V.: The Flexural Dynamics of Melting Ice Shelves, Annals of Glaciology, 54 (63), 1–10, doi:doi:10.3189/2013AoG63A256, 2013.

Mann, H. B.: Nonparametric Tests Against Trend, Econometrica, 13 (3), 245–259, doi:10.2307/1907187, 1945.

© Author(s) 2017. CC BY 4.0 License.

Marshall, G. J.: Half-Century Seasonal Relationships between the Southern Annular Mode and Antarctic Temperatures, Intl. Jour. of Clim., 27 (3), 373–83, doi:10.1002/joc.1407, 2007.

Marshall, G. J., Orr, A., Van Lipzig, N.P.M., and King, J.C.: The Impact of a Changing Southern Hemisphere Annular Mode on Antarctic Peninsula Summer Temperatures, J. of Climate, 19 (20), 5388–5404, 2006.

Mercer, J. H.: West Antarctic Ice Sheet and CO_2 Greenhouse Effect: A Threat of Disaster, Nature ,271 (January), 321–325, doi:10.1038/271321a0, 1978.

Morris, E. M., and Vaughan, D.G.: Spatial and Temporal Variation of Surface Temperature on the Antarctic Peninsula And The Limit of Viability of Ice Shelves, In: Antarctic Peninsula Climate Variability: Historical and Paleoenvironmental Perspectives, American Geophysical Union, 61–68, doi:10.1029/AR079p0061, 2013.

Mote, T., Anderson, M.R. , Kuivinen, K.C., and Rowe, M.C.: Passive Microwave-Derived Spatial and Temporal Variations of Summer Melt On the Greenland Ice Sheet, International Symposium On Remote Sensing of Snow and Ice, 17: 233–38, 1993.

Ridley, J.: Surface Melting on Antarctic Peninsula Ice Shelves Detected by Passive Microwave Sensors, Geoph. Res. Let., 20 (23), 2639–2642, doi:10.1029/93GL02611, 1993.

Rott, H., Rack, W., Nagler, T., and Skvarca, P.: Climatically Induced Retreat and Collapse of Northern Larsen Ice Shelf, Antarctic Peninsula, Annals of Glaciology 27, 86–92, doi:10.1017/S0260305500017262, 1998.

Rott, H., Rack, W., Skvarca, P., and De Angelis, H.: Northern Larsen Ice Shelf, Antarctica: Further Retreat after Collapse, Annals of Glaciology 34 (1), 277–82., doi: 10.3189/172756402781817716, 2002.

Scambos, T. A.: Glacier Acceleration and Thinning after Ice Shelf Collapse in the Larsen B Embayment, Antarctica, Geoph. Res. Let., 31 (18), doi:10.1029/2004GL020670, 2004.

Scambos, T.A., Hulbe, C., Fahnestock, M., and Bohlander, J.: The Link between Climate Warming and Break-up of Ice Shelves in the Antarctic Peninsula, J. Glaciology 46 (154), 516–530,doi:10.3189/172756500781833043, 2000.

Smith, L. C.: Melting of Small Arctic Ice Caps Observed from ERS Scatterometer Time Series, Geoph. Res. Let., 30 (20), doi:10.1029/2003GL017641, 2003.

Steiner, N., and Tedesco, M.: A Wavelet Melt Detection Algorithm Applied to Enhanced-Resolution Scatterometer Data over Antarctica (2000–2009),The Cryosphere, 8 (1), 25–40, doi:10.5194/tc-8-25-2014, 2014.

© Author(s) 2017. CC BY 4.0 License.

Tedesco, M.: Assessment and Development of Snowmelt Retrieval Algorithms over Antarctica from K-Band Spaceborne Brightness Temperature (1979–2008), Rem. Sen.of Env. ,113 (5), 979–997, doi:10.1016/j.rse.2009.01.009, 2009.

Tedesco, M., and Monaghan, A.J.: An Updated Antarctic Melt Record through 2009 and Its Linkages to High-Latitude and Tropical Climate Variability, Geophysical Research Letters, 36 (18), doi:10.1029/2009GL039186, 2009.

Tedesco, M., Abdalati, W., and Zwally, H. J.: Persistent Surface Snowmelt over Antarctica (1987–2006) from 19.35 GHz Brightness Temperatures, Geoph. Res. Let., 34 (18), doi:10.1029/2007GL031199, 2007.

Tedesco, M.: Snowmelt Detection over the Greenland Ice Sheet from SSM/I Brightness Temperature Daily Variations, Geoph. Res. Let., 34 (2), doi:10.1029/2006gl028466, 2007.

Torinesi, O., Fily, M., and Genthon, C.: Variability and Trends of the Summer Melt Period of Antarctic Ice Margins since 1980 from Microwave Sensors, J. of Climate, 16 (7), 1047–1060, 2003.

Trusel, L. D., Frey, K. E., and Das, S. B.: Antarctic Surface Melting Dynamics: Enhanced Perspectives from Radar Scatterometer Data, J. of Geoph. Res., 117 (F2), doi:10.1029/2011JF002126, 2012.

Trusel, L.D., Frey, K.D., Das, S.B., Kuipers-Munneke, P., and Van den Broeke, M.R.: Satellite-Based Estimates of Antarctic Surface Meltwater Fluxes, Geoph. Res. Let., 40 (23): 6148–6153. doi:10.1002/2013GL058138, 2013.

Turner, J., Colwell, S.R., Marshall, G.J., Lachlan-Cope, T.A., Carleton, A.M., Jones, P.D., Lagun, V., Reid, P.A., and Iagovkina, S.: Antarctic Climate Change during the Last 50 Years, Int. Journ. of Clim, 25 (3), 279–294, doi:10.1002/joc.1130, 2005.

Turner, J., Lu, H.,White, I., King, J.C., Phillips, T., Hosking, J.S., Bracegirdle, T.J., Marshall, G.J., Mulvaney, R., and Deb, P.: Absence of 21st Century Warming on Antarctic Peninsula Consistent with Natural Variability, Nature, 535 (7612), 411–415, doi:10.1038/nature18645, 2016.

Ulaby, F.T.., and Stiles, W.H.: The Active and Passive Microwave Response to Snow Parameters: 2. Water Equivalent of Dry Snow, J. of Geoph. Res.: Oceans, 85 (C2), 1045–1049, doi:10.1029/JC085iC02p01045, 1980.

Van Den Broeke, M. R., and Van Lipzig, N.P.M.,: Response of Wintertime Antarctic Temperatures to the Antarctic Oscillation: Results of a Regional Climate Model, in: Antarctic Peninsula Climate Variability: Historical and Paleoenvironmental Perspectives, American Geophysical Union, 43–58, 2003.

© Author(s) 2017. CC BY 4.0 License.

Van Den Broeke, M. R.: Strong Surface Melting Preceded Collapse of Antarctic Peninsula Ice Shelf, Geoph. Res. Let., 32 (12), doi:10.1029/2005GL023247, 2005.

van der Veen, C.J..: Fracture Mechanics Approach to Penetration of Surface Crevasses on Glaciers, Cold Regions Science and Technology 27 (1): 31–47. doi:10.1016/S0165-232X(97)00022-0, 1998.

Van Lipzig, N. P. M.: Precipitation, Sublimation, and Snow Drift in the Antarctic Peninsula Region from a Regional Atmospheric Model, J. of Geoph. Res., 109 (D24), doi:10.1029/2004JD004701, 2004.

Van Meijgaard, E., Van Ulft, L. H., Van de Berg, W. J., Bosveld, F. C., Van den Hurk, B., Lenderink, G., and Siebesma, A.P.: The KNMI Regional Atmospheric Climate Model RACMO Version 2.1., Koninklijk Nederlands Meteorologisch Instituut., http://a.knmi2.nl/knmi-library/knmipubTR/TR302.pdf, 2008.

Van Wessem, J. M., Ligtenberg, S. R. M., Reijmer, C. H., van de Berg, W. J., van den Broeke, M. R., Barrand, N. E.,Thomas, E. R. et al.: The Modelled Surface Mass Balance of the Antarctic Peninsula at 5.5 Km Horizontal Resolution, The Cryosphere Discussions, 9 (5), 5097–5136, doi:10.5194/tcd-9-5097-2015, 2015.

Vaughan, D. G., and Doake, C. S. M.: Recent Atmospheric Warming and Retreat of Ice Shelves on the Antarctic Peninsula, Nature, 379 (6563), 328–31, doi:10.1038/379328a0, 1996.

Vaughan, D. G.: Recent Trends in Melting Conditions on the Antarctic Peninsula and Their Implications for Ice-Sheet Mass Balance and Sea Level, Arctic, Antarctic, and Alpine Research, 38 (1), 147–152, 2006.

Vaughan, D. G.: West Antarctic Ice Sheet Collapse–the Fall and Rise of a Paradigm, Climatic Change, 91 (1–2), 65–79, 2008.

Wallace, J. M., and Hobbs, P.V.: Hypsometric Equation,in: Atmospheric Science: An Introductory Survey, Academic Press, Cambridge, MA, 55–57, 1977.

Weertman, J.:Can a Water-Filled Crevasse Reach the Bottom Surface of a Glacier., IASH Publ 95, 139–145., 1973

Wilks, D.S.: Statistical Methods in the Atmospheric Sciences: An Introduction. International Geophysics, Elsevier Science, Amsterdam, Netherlands,1995.

Wismann, V.: Monitoring of Seasonal Snowmelt on Greenland with ERS Scatterometer Data, IEEE Transactions on Geoscience and Remote Sensing, 38 (4), 1821–1826, doi:10.1109/36.851766, 2000.

© Author(s) 2017. CC BY 4.0 License.

Zwally, H. J., Giovinetto, M. B., Beckley, M. A., and Saba, J. L.: Antarctic and Greenland Drainage Systems, GSFC Cryospheric Sciences Laboratory, 2012.

Zwally, H. Jay, Abdalati, W., Herring T., Larson, K., Saba, J., and Steffen, K.: Surface Melt-Induced Acceleration ofGreenland Ice-Sheet Flow, Science ,297 (5579), 218–222., 2002.

Zwally, H. J., and Fiegles, S.: Extent and Duration of Antarctic Surface Melting, J. of Glaciology, 40, 463–476, 1994.

The Cryosphere Discuss., https://doi.org/10.5194/tc-2017-253
Manuscript under review for journal The Cryosphere
Discussion started: 22 December 2017
© Author(s) 2017. CC BY 4.0 License.

The Cryosphere Discussions
Open Access
EGU

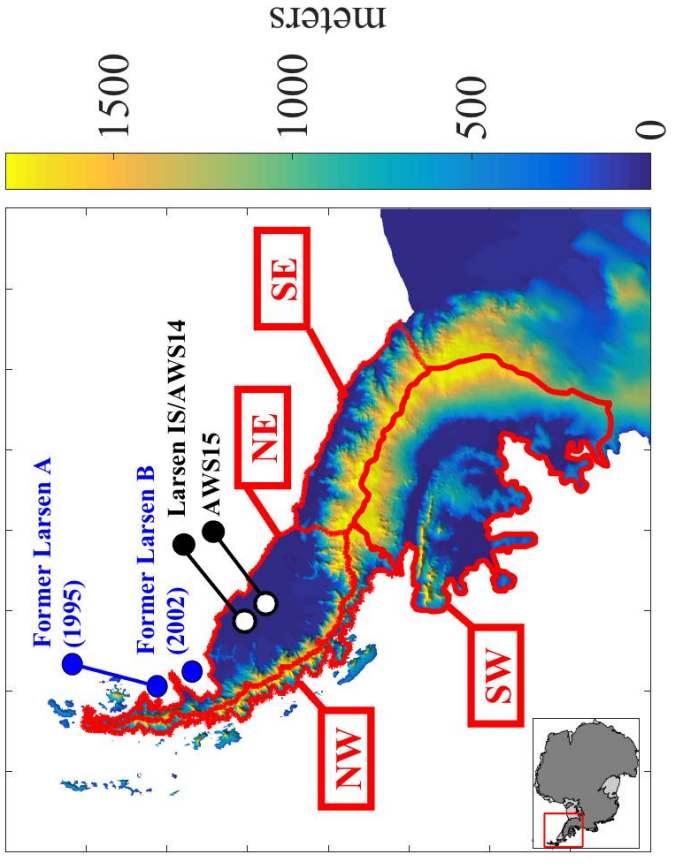

Figure 1: Full MAR domain showing topographic relief, former ice shelves with dates of collapse, locations of automatic weather stations and basins corresponding to SW (basin 24) NW (basin 25) NE (basin 26), SE (basin 27) from Zwally,et. al. 2012

The Cryosphere Discuss., https://doi.org/10.5194/tc-2017-253
Manuscript under review for journal The Cryosphere
Discussion started: 22 December 2017
© Author(s) 2017. CC BY 4.0 License.

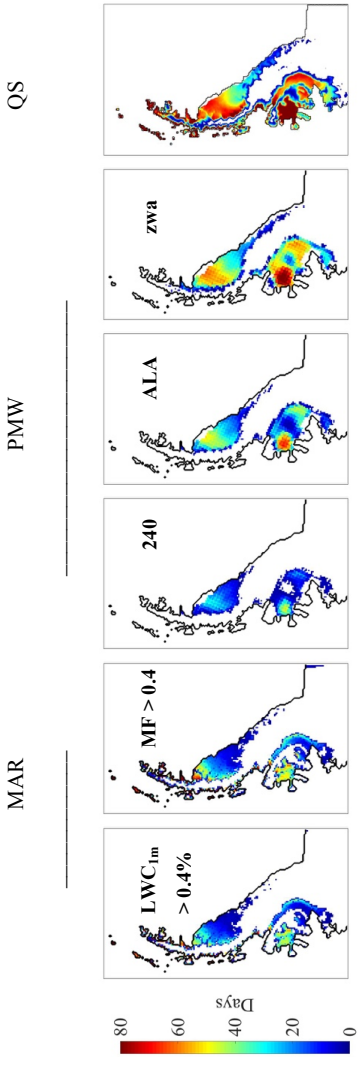

Figure 2: Average number of melt days from multiple sources (a) MAR, Liquid Water Content > 0.4% for three consecutive days. (b) MAR Total Melt Flux >0. 4 mmwe for 1 day or more. Satellite-based: (c) PMW 240 algorithm (d) PMW ALA (e) PMW Zwa (f) QuikSCAT. All satellite-based estimates include a melt day only when part of a sustained three-day period of melt. All averages are taken from the 2000-2009 period to retain consistency with the availability of QuikSCAT data

The Cryosphere Discuss., https://doi.org/10.5194/tc-2017-253
Manuscript under review for journal The Cryosphere
Discussion started: 22 December 2017
© Author(s) 2017. CC BY 4.0 License.

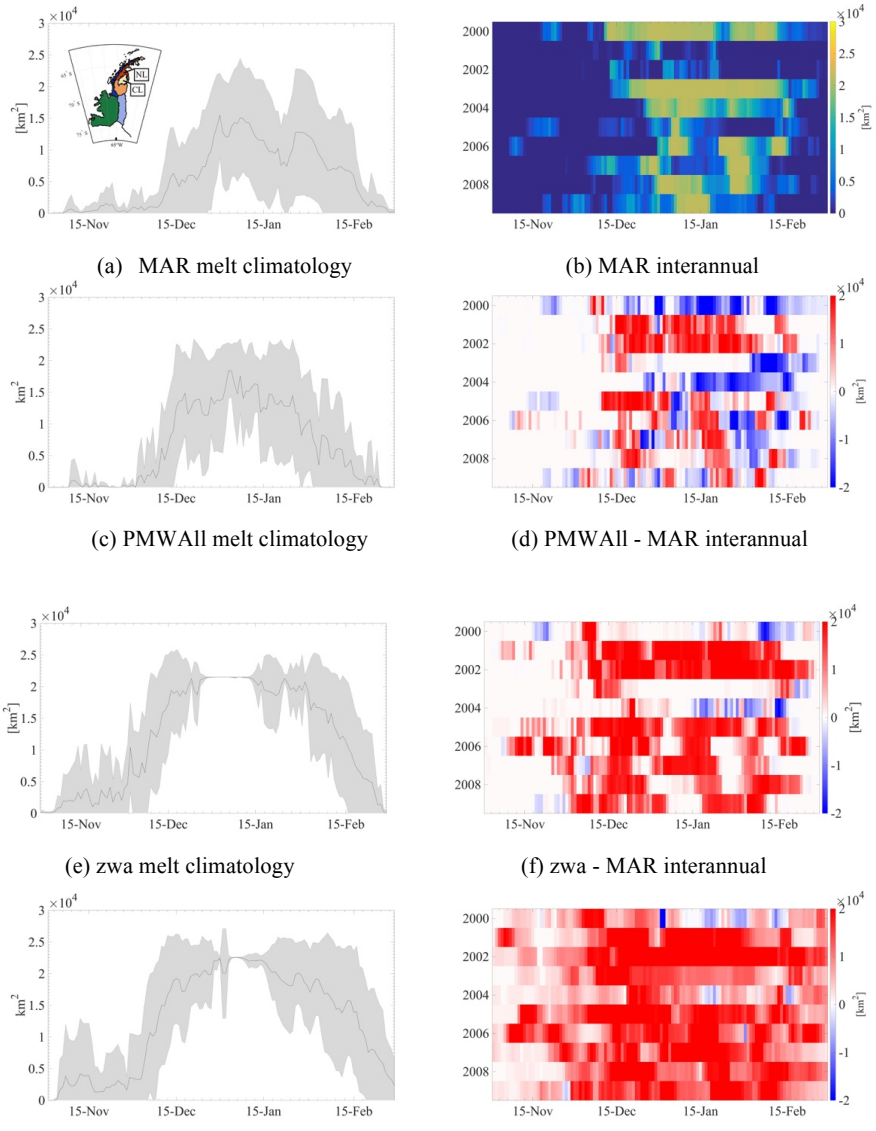

Figure 3: CL-region, described in text and shown in inset in for (a), average and inter-annual melt occurrence in MAR, PMW and QuikSCAT data. (a) $MF_{0.4}$ melt extent climatology with one standard deviation shown in grey envelope (b) melt extent for $MF_{0.4}$ from 1999-2009 (c) melt climatology PMW All (d) interannual difference melt extent PMWAll - MAR (e) melt climatology PMW zwa (f) interannual difference in melt extent PMWzwal – MAR (g) melt climatology QuikSCAT ft3 (h) interannual difference in melt extent QuikSCAT ft3 - MAR

The Cryosphere Discuss., https://doi.org/10.5194/tc-2017-253
Manuscript under review for journal The Cryosphere
Discussion started: 22 December 2017
© Author(s) 2017. CC BY 4.0 License.

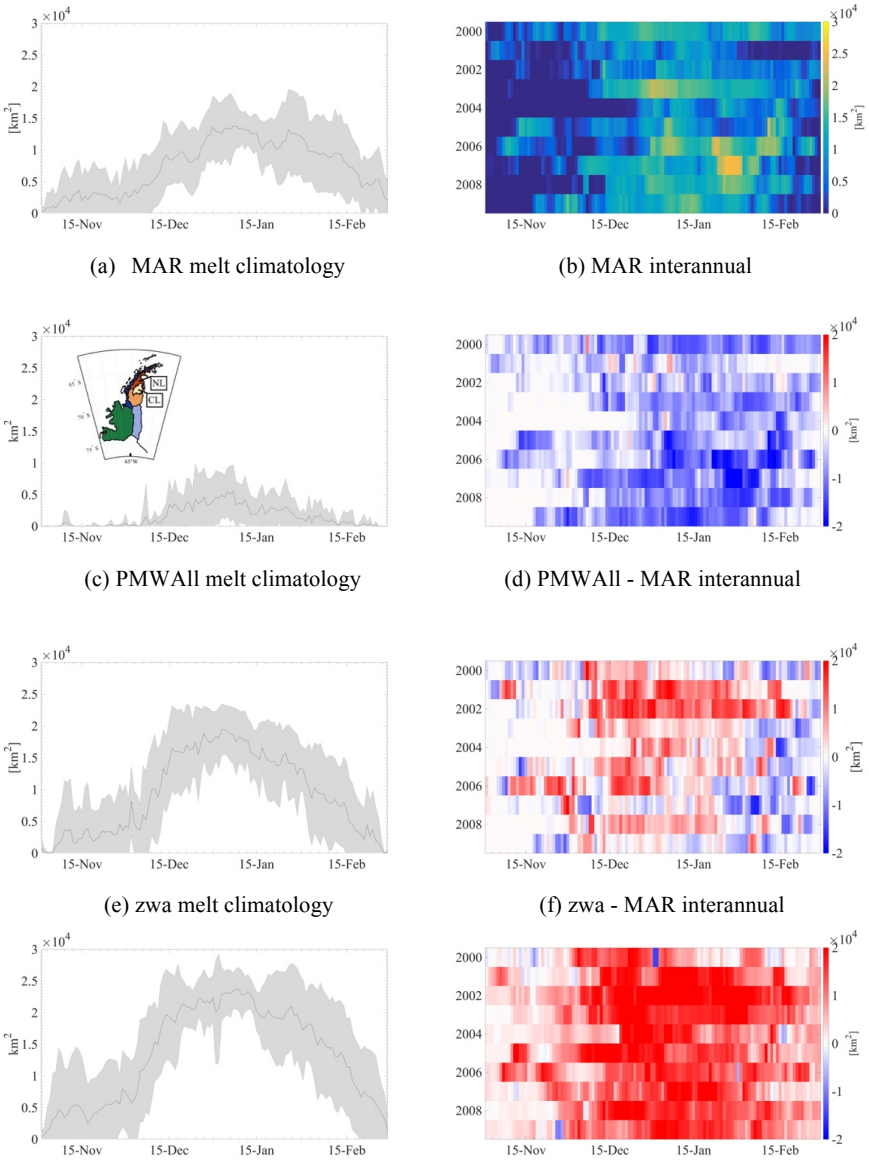

Figure 4: NL-region, described in text and shown inset in (c), average and inter-annual melt occurrence in MAR, PMW and QuikSCAT data. (a) $MF_{0.4}$ melt extent climatology with one standard deviation shown in grey envelope (b) melt extent for $MF_{0.4}$ from 1999-2009 (c) melt climatology PMW All (d) interannual difference melt extent PMWAll - MAR (e) melt climatology PMW zwa (f) interannual difference in melt extent PMWzwal – MAR (g) melt climatology QuikSCAT ft3 (h) interannual difference in melt extent QuikSCAT ft3 - MAR

The Cryosphere Discuss., https://doi.org/10.5194/tc-2017-253
Manuscript under review for journal The Cryosphere
Discussion started: 22 December 2017
© Author(s) 2017. CC BY 4.0 License.

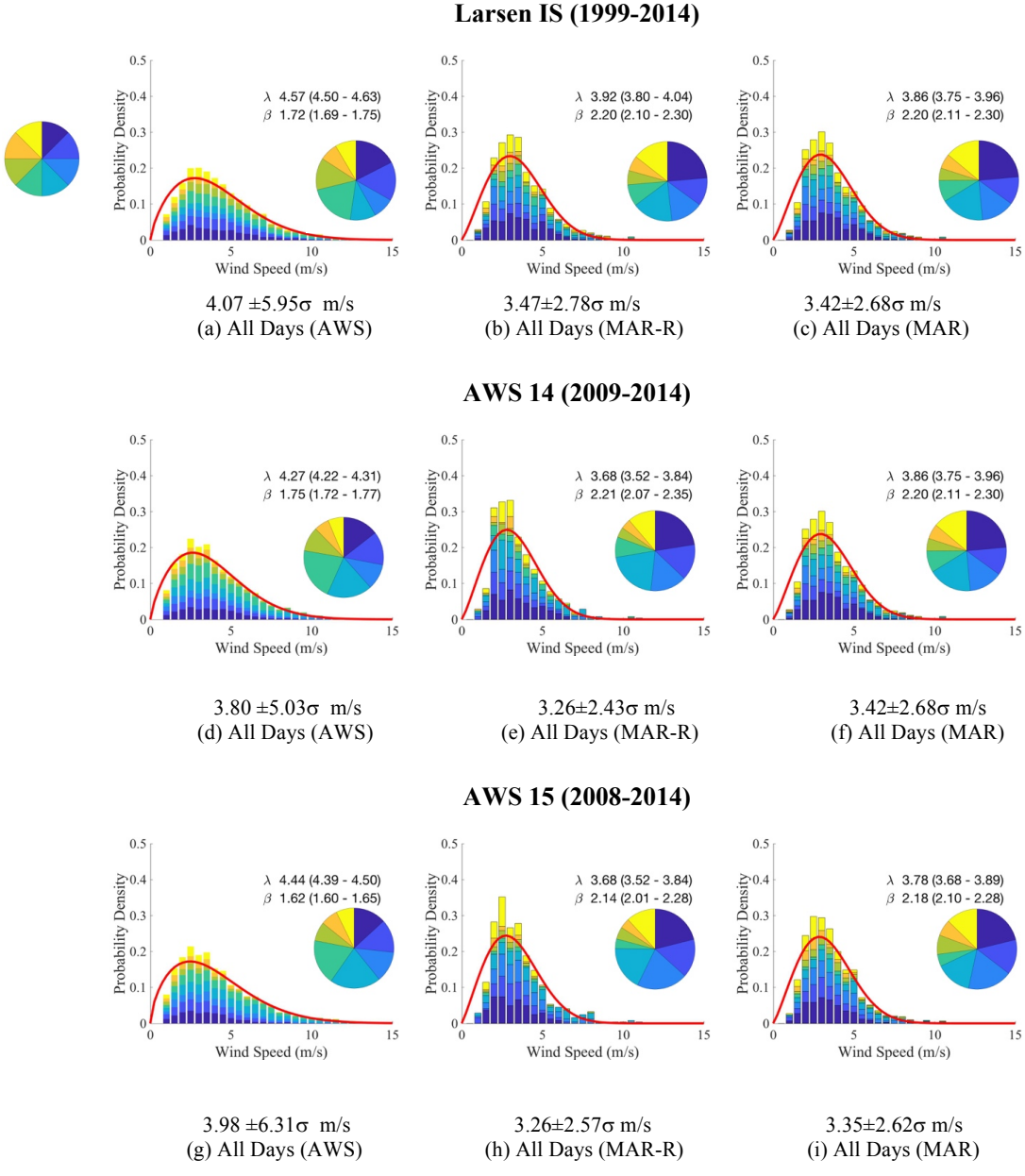

Figure 5: Probability distribution (y-axis) of summer (DJF) wind speeds (x-axis) with wind speed direction proportions shown in each inset. Wind directions corresponding to instet colors shown in 45° increments in inset left of (a). Curve shows best-fit Weibull curve with parameters for shape (β) and scale (λ ,m/s). Datasets are for AWS data (left column), MAR outputs restricted to AWS availability (middle column) and MAR data for the 2001-2014 period (right column). Shown for (a) Larsen, AWS (b) Larsen, MAR at AWS availability (c) Larsen, MAR full period (d) AWS 14, (e) AWS 14, MAR at AWS availability (f) AWS 14, MAR full period (g) AWS 15, AWS (h) AWS 15, MAR at AWS availability (i) AWS 15, MAR full period. Values shown below figures are expected values from the Weibull distribution

The Cryosphere Discuss., https://doi.org/10.5194/tc-2017-253
Manuscript under review for journal The Cryosphere
Discussion started: 22 December 2017
© Author(s) 2017. CC BY 4.0 License.

	Northerly	Southerly	Easterly	Westerly
DJF All Days				
Where MAR shows wind direction				
MAR wind direction percentage	55.6%	44.4%	63.9%	36.3%
MAR expected wind speed [m/s]	3.49(±3.12)	4.21(±4.83)	3.75(±3.09)	4.04(±5.69)
AWS expected wind speed [m/s]	3.82(±5.23)	5.10(±9.14)	4.41(±6.87)	4.44(±8.73)
Where AWS shows wind direction				
AWS wind direction percentage	51.2%	48.8%	54.5%	45.5%
MAR expected wind speed [m/s]	4.04(±5.31)	3.72(±3.07)	3.48(±2.37)	4.43(±6.26)
AWS expected wind speed [m/s]	4.52(±8.33)	4.39(±6.98)	3.90(±4.77)	5.22(±11.03)
Temperature biases				
Avg T2m Bias (MAR - AWS)	0.58°C	0.77°C	0.43°C	0.76°C
Max T2m Bias (MAR - AWS)	-2.21°C	-1.11°C	-1.75°C	-2.42°C
Temperature bias where Ts > 0°C				
Avg T2m Bias (MAR - AWS)	-1.25°C	-1.42°C	-1.32°C	-1.29°C
Max T2m Bias (MAR - AWS)	-2.80°C	-2.40°C	-2.84°C	-3.04°C
DJF, MAR reports melt				
MAR wind direction	59.5%	40.5%	62.8%	37.2%
AWS wind direction	55%	45%	56.7%	43.3%
Temperature biases				
Avg T2m Bias (MAR - AWS)	0.28°C	0.18°C	0.25°C	0.24°C
Max T2m Bias (MAR - AWS)	-0.78°C	-0.41°C	-0.73°C	-0.43°C
Temperature bias where Ts > 0°C				
Avg T2m Bias (MAR - AWS)	-0.69°C	-0.76°C	-0.47°C	-0.63°C
Max T2m Bias (MAR - AWS)	-1.06°C	-0.92°C	-1.31°C	-0.64°C

Table 1: Proportions for wind direction and associated temperature biases at the Larsen Ice Shelf AWS station from 2000-2009 restricted to the summer season (DJF)

The Cryosphere Discuss., https://doi.org/10.5194/tc-2017-253
Manuscript under review for journal The Cryosphere
Discussion started: 22 December 2017
© Author(s) 2017. CC BY 4.0 License.

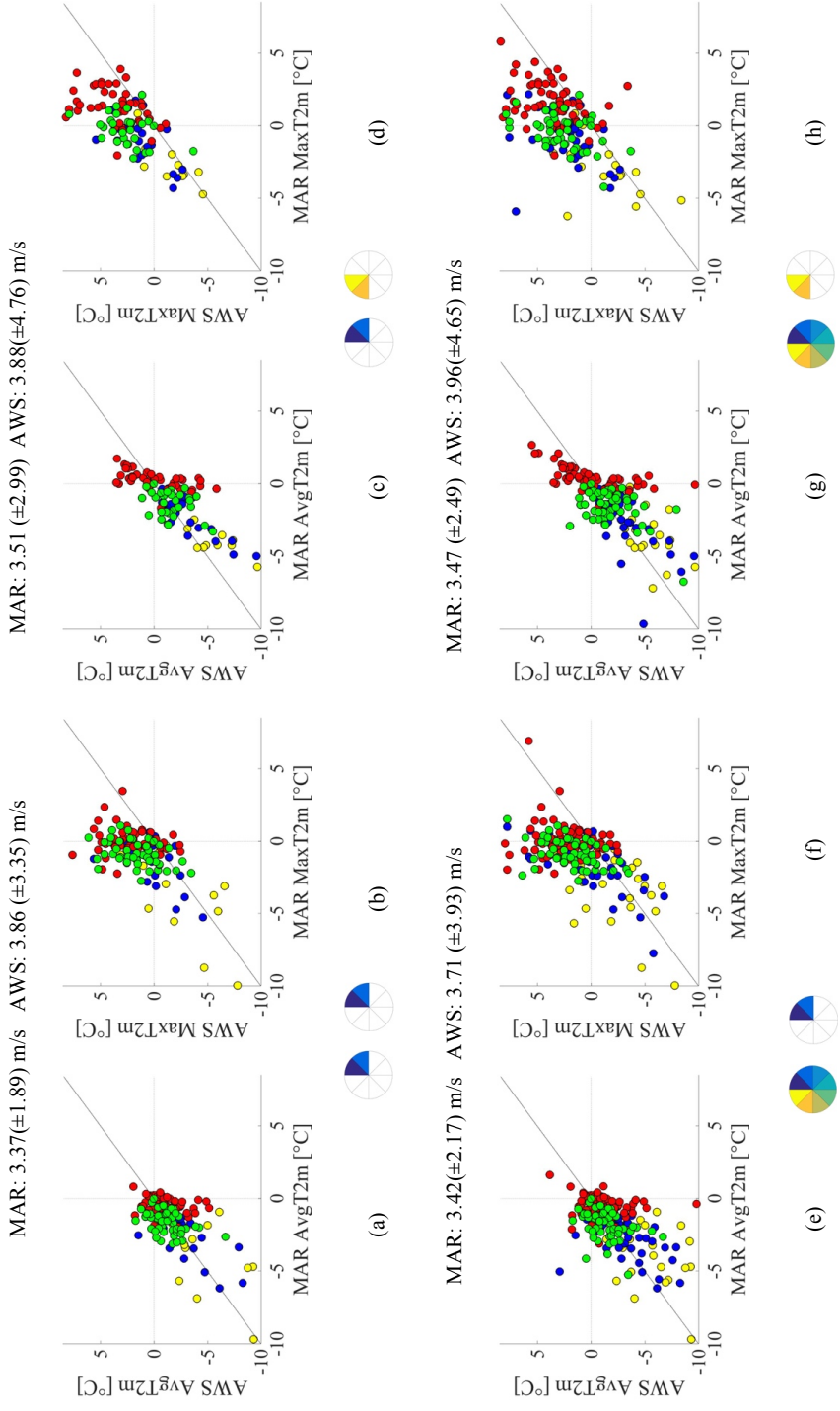

Figure 6: MAR vs AWS temperatures at the Larsen Ice Shelf AWS station for DJF from 2001-2009 for wind biases AWS -> MAR shown by pie charts (when AWS data is available). Red shows days where MAR shows melt. Blue shows "QSEx" days, i.e. when QuikSCAT reports melt (and MAR does not), Cyan indicates "PMWEx" when PMWAll shows melt and MAR does not. Green indicates when PMWEx an QSEx both report melt (and MAR does not). Yellow (only shown for g,h) indicates all other days for completeness. Northeasterly agreement (case 1) (a) AvgTs (b) MaxTs. Northeasterly AWS winds reported as northwesterly in MAR (case 2) (c) AvgTs (d)MaxTs, All wind directions in AWS reported as northeasterly in MAR (e) AvgTs (f) MaxTs

The Cryosphere Discuss., https://doi.org/10.5194/tc-2017-253
Manuscript under review for journal The Cryosphere
Discussion started: 22 December 2017
© Author(s) 2017. CC BY 4.0 License.

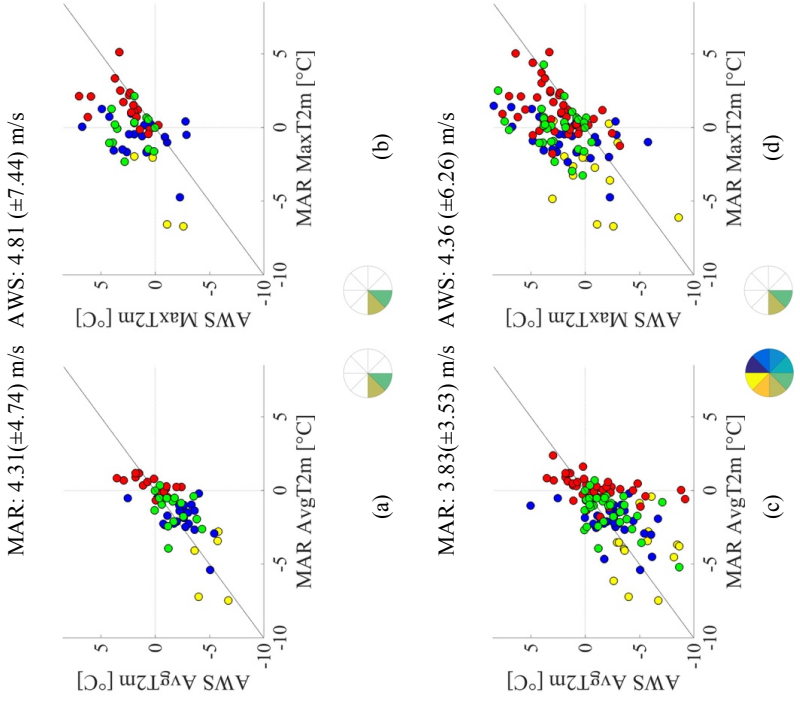

Figure 7: MAR vs AWS temperatures at the Larsen Ice Shelf AWS station for DJF from 2001-2009 for wind biases AWS -> MAR shown by pie charts (when AWS data is available). Red shows days where MAR shows melt. Blue shows "QSEx" days, i.e. when QuikSCAT reports melt (and MAR does not), Cyan indicates "PMWEx" when PMWAll shows melt and MAR does not. Green indicates when PMWEx an QSEx both report melt (and MAR does not). Yellow (only shown for g,h) indicates all other days for completeness. Southwesterly wind direction agreement (a) AvgTs (b) MaxTs, All wind directions in AWS which are reported as southwesterly in MAR (c) AvgTs (d)MaxTs,

The Cryosphere Discuss., https://doi.org/10.5194/tc-2017-253
Manuscript under review for journal The Cryosphere
Discussion started: 22 December 2017
© Author(s) 2017. CC BY 4.0 License.

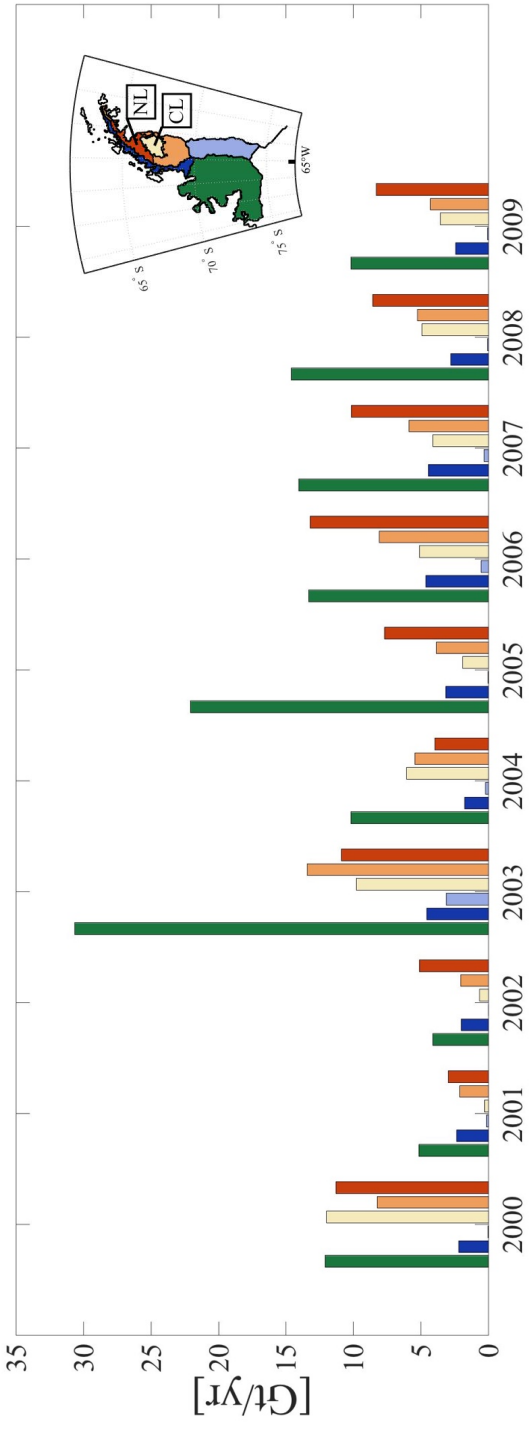

Figure 8: Annual meltwater production from MAR [Gt/yr] shown for masks shown in inset ('2001' corresponds to the meltwater from July,2000-June,2001). NW, SW, SE basins are kept intact as in Fig. 1. NE basin is divided into the NL mask, the CL mask and the remaining portion of the NE basin (NE – (CL+NL)). The CL and NL masks are described in text